EUROPEAN RESPIRATORY *journal*

FLAGSHIP SCIENTIFIC JOURNAL OF ERS

Early View

Original article

Cyclophilin Inhibitors Restrict Middle East Respiratory Syndrome Coronavirus *Via* Interferon λ *In Vitro* And In Mice

Lucie Sauerhering, Alexandra Kupke, Lars Meier, Erik Dietzel, Judith Hoppe, Achim D. Gruber, Stefan Gattenloehner, Biruta Witte, Ludger Fink, Nina Hofmann, Tobias Zimmermann, Alexander Goesmann, Andrea Nist, Thorsten Stiewe, Stephan Becker, Susanne Herold, Christin Peteranderl

Please cite this article as: Sauerhering L, Kupke A, Meier L, *et al*. Cyclophilin Inhibitors Restrict Middle East Respiratory Syndrome Coronavirus *Via* Interferon λ *In Vitro* And In Mice. *Eur Respir J* 2020; in press (https://doi.org/10.1183/13993003.01826-2019).

This manuscript has recently been accepted for publication in the *European Respiratory Journal*. It is published here in its accepted form prior to copyediting and typesetting by our production team. After these production processes are complete and the authors have approved the resulting proofs, the article will move to the latest issue of the ERJ online.

Cyclophilin Inhibitors Restrict Middle East Respiratory Syndrome Coronavirus Via Interferon λ In Vitro And In Mice

Lucie Sauerhering[1], Alexandra Kupke[1], Lars Meier[1], Erik Dietzel[1], Judith Hoppe[2], Achim D. Gruber[2], Stefan Gattenloehner[3], Biruta Witte[4], Ludger Fink [5], Nina Hofmann[6], Tobias Zimmermann[6], Alexander Goesmann[6], Andrea Nist[7], Thorsten Stiewe[7,8], Stephan Becker[1*], Susanne Herold[9*], Christin Peteranderl[9*]

* equal contribution

[1]Institute of Virology, Philipps University of Marburg, German Center for Infection Research (DZIF), TTU Emerging Infections, Marburg, Germany

[2] Department of Veterinary Pathology, Free University Berlin, Berlin, Germany

[3]Department of Pathology, University Hospital of Giessen, Giessen, Germany

[4]Department of General and Thoracic Surgery, University Hospital of Giessen, Giessen, Germany

[5]Institut für Pathologie und Zytologie, Wetzlar, Germany

[6]Bioinformatics and System Biology, University of Giessen, Giessen, Germany

[7]Genomics Core Facility, Philipps-University of Marburg, Marburg, Germany

[8]Institute of Molecular Oncology, Universities of Giessen and Marburg Lung Center, German Center for Lung Research (DZL), Marburg, Germany

[9]Department of Internal Medicine II, University of Giessen and Marburg Lung Center (UGMLC), Member of the German Center for Lung Research (DZL), Giessen, Germany

Corresponding author

Christin Peteranderl, PhD

Universities Giessen & Marburg Lung Center, Department of Internal Medicine II

Klinikstr. 36, D-35392 Giessen, Germany

Phone: +49-641-985-42138

Email: Christin.Peteranderl@innere.med.uni-giessen.de

Take Home

The cyclophilin inhibitors Cyclosporin A and Alisporivir activate host innate immunity by induction of interferon lambda via activation of IRF1 in human lung epithelial cells and *in vivo*, resulting in a significant inhibition of MERS-CoV.

This article has an online data supplement.

Sequencing data are available at Array Express, accession number E-MTAB-8222.

Abstract

Rationale

While severe coronavirus infections, including Middle East respiratory syndrome coronavirus (MERS-CoV) cause lung injury with high mortality rates, protective treatment strategies are not approved for clinical use.

Objectives

We elucidated the molecular mechanisms by which the cyclophilin inhibitors Cyclosporin A (CsA) and Alisporivir (ALV) restrict MERS-CoV to validate their suitability as readily-available therapy in MERS-CoV infection.

Methods

Calu-3 cells and primary human alveolar epithelial cells (hAEC) were infected with MERS-CoV and treated with CsA or ALV or inhibitors targeting cyclophilin inhibitor-regulated molecules including Calcineurin, NFAT, or MAP kinases. Novel CsA-induced pathways were identified by RNA sequencing and manipulated by gene knockdown or neutralizing antibodies. Viral replication was quantified by qRT-PCR and $TCID_{50}$. Data were validated in a murine MERS-CoV infection model.

Results

CsA and ALV both reduced MERS-CoV titers and viral RNA replication in Calu-3 and hAEC improving epithelial integrity. While neither Calcineurin nor NFAT inhibition reduced MERS-CoV propagation, blockade of c-Jun N-terminal kinase diminished infectious viral particle release but not RNA accumulation. Importantly, CsA induced interferon regulatory factor 1 (IRF1), a pronounced type-III-interferon (IFNλ) response

and expression of antiviral genes. Down-regulation of IRF1 or IFNλ increased MERS-CoV propagation in presence of CsA. Importantly, oral application of CsA reduced MERS-CoV replication *in vivo*, correlating with elevated lung IFNλ levels and improved outcome.

Conclusions

We provide evidence that cyclophilin inhibitors efficiently decrease MERS-CoV replication *in vitro* and *in vivo* via upregulation of inflammatory, antiviral cell responses, in particular IFNλ. CsA might therefore represent a promising candidate to treat MERS-CoV infection.

Introduction

Middle East respiratory syndrome coronavirus (MERS-CoV) emerged in 2012 in Saudi Arabia [1] and led to recurring human infections with more than 2,500 laboratory-confirmed cases and high case fatality rates of about 35% [2]. In *ex vivo* infection of human lung tissue, MERS-CoV targets bronchial and alveolar epithelial cells (AEC) and leads to a detachment and apoptosis of AEC [3]. Recent reports analyzing autopsy material of deceased MERS-CoV-infected patients showed MERS-CoV antigen in AEC and epithelial multinucleated syncytial cell conglomerates *in vivo* [4, 5]. Accordingly, severe human infection presents as pneumonia with progression to acute respiratory distress syndrome [4, 5].

To date, no vaccine or specific treatment for MERS-CoV - or the recently ongoing pandemic caused by the novel severe acute respiratory syndrome CoV 2 (SARS-CoV-2) - is approved and therapy relies on supportive measures only [2, 6]. While *in vitro* studies and experiments in non-human primates demonstrated benefits of a combination of type-I-interferon and antiviral compounds including ribavirin against MERS-CoV [7–9], results from retrospective patient cohorts applying similar treatment regimens remain controversial [10–12]. Cyclosporin A (CsA) has been found to inhibit several human-pathogenic CoV in cell lines originating from kidney or liver epithelia [13–16]. However, the molecular mechanisms by which CsA affects CoV, including MERS-CoV, particularly in its primary target cells, the pulmonary epithelium, remain elusive. Moreover, preclinical studies addressing the effect of CsA or related compounds on MERS-CoV replication *in vivo* have been lacking to date.

CsA is known to block the peptidyl-prolyl cis-trans isomerase (PPI) activity of cyclophilins that is involved in diverse cellular processes (e.g. protein folding, 17).

Additionally, CsA forms together with cyclophilin A (CypA) and calcineurin (CnA) a ternary complex which blocks the CnA-dependent activation of NFAT (nuclear factor of activated T-cells), a process which accounts for the immunosuppressive effect of CsA [18]. In addition, CsA has also been shown to inhibit the MAP kinases JNK (c-Jun N-terminal kinase) and p38 [19, 20].

Here, we aimed to elucidate the distinct signaling pathways by which CsA affects MERS-CoV in clinically relevant models such as primary human AEC and a murine MERS-CoV infection model [21, 22]. We demonstrate that CsA blocks MERS-CoV infectious particle egress, which is dependent on JNK. Moreover, we for the first time provide evidence that CsA triggered the activation of an antiviral defense state in lung epithelial cells. We show that CsA is a potent inducer of Interferon regulatory factor 1 (IRF1), type-III-IFN (IFNλ) and multiple interferon-stimulated genes (ISGs). Additionally, we demonstrate that oral application of CsA induced a robust IFNλ response *in vivo* and, importantly, significantly reduced MERS-CoV replication and improved disease progression in infected mice.

Materials and Methods

MERS-CoV infection

Experiments with MERS-CoV were performed under biosafety level 4 conditions at the Institute of Virology, Philipps-University of Marburg, Germany. Human alveolar epithelial cells (hAEC) were isolated and cultured as previously described [23]. Human lung tissue was obtained from patients who underwent lobectomy after informed written consent (Departments of Pathology and Surgery, University of

Giessen, approved by the University of Giessen Ethics Committee; Az.58/15). Calu-3 or hAEC were infected at a multiplicity of infection (MOI) of 0.1 diluted in DMEM/F12 without FCS at 37°C for 1 h. Cells were washed with DMEM/F12 with 10% FCS and supplemented with stimulatory/ inhibitory reagents as indicated. 24 h after infection (pi) cells were processed for quantitative PCR (Maxima-SYBR/ROX qPCR-Mastermix, Thermo Fisher) and supernatant was harvested for virus titration as described previously [24].

In vivo transduction and infection

All animal experiments were performed in accordance with the German animal protection laws and were authorized by the regional authorities (G73/2017). C57BL/6 mice were purchased from Charles River Laboratories and housed under pathogen-free conditions. Mice were intratracheally inoculated with Adenovirus-hDPP4-mCherry (cloned at ViraQuest Inc.) as described [21, 25]. Five days post transduction, mice were infected intranasally with $1.5x10^5$ $TCID_{50}$/ml MERS-CoV (EMC/2012). 50 mg/kg/day CsA diluted in DMSO or DMSO alone were mixed with a nut/chocolate-creme, and offered to the mice for voluntary uptake. Uptake was controlled daily. CsA feeding started 2 days before MERS-CoV challenge. Mice were sacrificed 4 or 7 days post MERS-CoV infection.

RNA-seq analysis

RNA integrity was assessed on an Experion StdSens RNA Chip (Bio-Rad). RNA-seq libraries were prepared using the TruSeq Stranded mRNA Library Prep kit (Illumina). Libraries were quantified on a Bioanalyzer (Agilent Technologies) and sequenced on an Illumina HiSeq 1500 platform, rapid-run mode, single-read 50 bp (HiSeq SR Rapid Cluster Kit v2, HiSeq Rapid SBS Kit v2, 50 cycles) according to the manufacturer's

instructions. Quality control of RNA-seq reads was performed using the FastQC command line tool version 0.11.7. Reads were aligned using STAR version 2.7.0d to an index based on hg38 human genome version. Gene-specific read counts based on hg38 UCSC gene annotations were extracted using FeatureCounts from the Subread package version 1.6.3. Resulting read counts were imported into R. Detection of differentially expressed genes was done using DESeq2 version 1.22.1. Subsequent data analysis and visualization was done with custom R scripts. GO overrepresentation analysis was performed using the enrichGO function of the clusterProfiler package version 3.10.1. Sequencing data are available at Array Express, accession number E-MTAB-8222.

Statistics

All data are given as mean ± SEM. Statistical significance was analyzed by unpaired two-tailed Student's t-test or by 1-way ANOVA and post-hoc multi-comparison tests as indicated in the respective figures. A P value of less than 0.05 was considered significant. *P < 0.05; **P < 0.01; ***P < 0.005.

Further experimental details can be found in the Online Supplement.

Results

Cyclosporin A (CsA) inhibits MERS-CoV replication and release in lung epithelia

To address the previously proposed antiviral activity of CsA in clinically relevant cells, we infected the human bronchial epithelial cell line Calu-3 and primary human alveolar epithelial cells (hAEC) with MERS-CoV and analyzed intracellular viral RNA and infectious particle release in presence of DMSO or CsA (Figure 1). In both Calu-3 and hAEC, CsA treatment led to a >95% decrease of viral RNA (Figure 1A) and a reduction of viral titers in the supernatant by 2.6-2.8 $\log_{10}$, respectively (Figure 1B). Interestingly, and in accordance with reports from autopsy material of MERS-CoV patients [4], MERS-CoV-infected Calu-3 and primary hAEC both showed apoptotic cell loss and formation of multinucleated cell foci (Figure 1C). Addition of CsA reduced cell foci formation and significantly reduced apoptosis induction (Figure 1C, D). In line, both CFTR (cystic fibrosis transmembrane conductance regulator; Figure 1E) and ENaCβ (epithelial sodium channel beta; Supplement Fig.E1) protein expression was improved after addition of CsA to MERS-CoV-infected Calu-3. Moreover, epithelial structural integrity and ability for vectorial water transport were reduced in MERS-CoV-infected control cells and significantly improved to normal levels in MERS-CoV-infected, CsA-treated cells (Figure 1F, G).

CsA treatment affects MERS-CoV infection via CypA- and MAPK-signaling pathways

CsA is known to act via multiple signaling pathways including cyclophilin PPIase activity, the CnA-NFAT axis as well as MAP kinase signaling [17–20]. Using specific inhibitors, we aimed to interfere with CsA-affected pathways to identify relevant molecular signaling events involved in the CsA-mediated reduction of MERS-CoV infection. Inhibition of CnA by its specific inhibitor calcineurin inhibitory peptide (CIP), as well as inhibition of the downstream transcription factor NFAT resulted in minor, statistically non-significant changes in MERS-CoV viral titers in both Calu-3 and hAEC (Figure 2A, B). The non-immunosuppressive derivate of CsA, Alisporivir (ALV), that binds the PPIase but does not induce ternary complex formation of CypA with CnA, reduced viral titers to a similar extent as CsA, suggesting that the CypA-PPIase activity elicits the restrictive effect on MERS-CoV replication rather than ternary complex-mediated signaling events. Moreover, ALV reduced cell foci formation and loss of epithelial integrity to a similar extent as CsA (Supplement Fig. E2). Applying specific MAPK inhibitors against JNK and p38, we revealed that inhibition of the MAP kinase JNK, but not of p38 reduced MERS-CoV titers in both Calu-3 and hAEC (Figure 2A, B). However, neither inhibition of CnA-dependent signaling nor inhibition of JNK or p38 could reproduce the CsA-induced attenuation of MERS-CoV RNA accumulation. In addition, JNK inhibition had no positive effect on cell foci formation or epithelial integrity after MERS-CoV infection (Supplement Fig. E3). These data suggest a role for JNK activity late in MERS-CoV replication, where adverse effects on epithelial integrity are still displayed while viral release is blocked. Of note, application of ALV resulted in a strong reduction of MERS-CoV RNA levels similar to CsA (Figure 2C, D). Together, these results indicate that a CsA-induced, CypA-

dependent effect has major impact on early replication steps of MERS-CoV, strongly reducing viral RNA accumulation, even prior to virus release, independently of CnA, NFAT or JNK.

CsA treatment evokes an interferon-driven antiviral state in lung epithelial cells

Our data suggest that, as opposed to its well-known CnA/NFAT-mediated immune-suppressive effects on immune cells, CsA might evoke an antiviral state in human lung epithelial cells. To identify the underlying mechanism, we performed RNA sequencing analysis on CsA- versus DMSO-treated Calu-3 cells. Of note, analysis of enriched gene sets based on GO terms revealed that the most significantly upregulated biological processes after CsA treatment included responses to viruses and, importantly, antiviral interferon responses (Figure 3A). In line with these results, both the type-I-IFN gene *IFNB* and type-III-IFN genes *IFNL1* and *IFNL2* were among the top-50, or, in case of *IFNL1*, top-10 most upregulated genes in CsA-treated cells (Figure 3B, C). Many of the upregulated genes were known interferon-stimulated genes (ISGs), including *MX*1, *MX2*, *OAS1*, *OAS2*, *IFIT1*, *IFIT2*, *IFIT3*, *LAMP3*, *BST2/tetherin*, *RSAD2/viperin* or *CXCL10* (Figure 3B).

To validate our results, we analyzed mRNA expression of both type-I and type-III-IFN by qRT-PCR in CsA-stimulated or DMSO-treated Calu-3 cells. We found a moderate upregulation of *IFNB* (up to 57 fold change over mock) and no significant induction of *IFNA* (Figure 4A, upper panels). However, we revealed a strong induction of *IFNL1* and *IFNL2/3* mRNAs (between 150 and 387 fold change over unstimulated mock control, respectively; Figure 4A, lower panels). Quantification of IFNλ1 and IFNλ3 protein release from cell culture supernatants by ELISA demonstrated a robust induction upon CsA addition as early as 12 h after CsA

treatment, reaching peak values of 4222 ± 890 ng protein ml^{-1} at 48 to 56 h after CsA application (Figure 4B). Similarly, treatment with ALV induced robust IFNλ release within reaching a similar maximum release of IFNλ after 72 h (Supplement Fig.E4). We next validated the CsA-induced upregulation of ISGs and confirmed an increased expression of selected ISGs including *MxA*, *PKR*, *OAS1*, *IFIT1*, *IFIT2*, *IFIT3*, *Bst2/tetherin*, *RSAD2/viperin* and *XAF1* upon 18 h treatment with CsA compared to vehicle-treated control cells (Figure 4C). These data indicate that CsA treatment mounts a distinct interferon-driven antiviral response in lung epithelial cells.

IFNλ-induction is mediated by IRF1 upon CsA treatment in lung epithelial cells

To better understand the transcriptional programs leading to IFNλ induction in CsA-treated cells, we analyzed the regulation of interferon regulatory factors (IRFs). Our data reveal significant upregulation of *IRF1* mRNA levels upon CsA treatment, but not of *IRF3*, *IRF7* or *IRF9* (Figure 5A). IRF1 is known to be a specific activator of *IFNL* gene expression [26]. Accordingly, we identified a significantly increased number of IRF1-expressing cells in CsA-stimulated Calu-3 cells by immunofluorescence (Figure 5B). In line, *IRF1* siRNA knockdown significantly reduced *IFNL* mRNA levels in CsA treated Calu-3 cells (Figure 5C). Accordingly, *IRF1* knockdown inhibited IFNλ release by more than 75 % as compared to control (Figure 5D).

Inhibition of the IRF1-IFNλ signaling axis counteracts the MERS-CoV restrictive effect of CsA

To understand the extent to which the inhibition of MERS-CoV propagation in CsA treated cells was mediated by IRF1-mediated production of IFNλ, we performed knockdown of *IRF1* or neutralized cell-free IFNλ, respectively. Our data demonstrated that silencing of *IRF1* but not treatment by control siRNA lead to a significant increase in MERS-CoV released viral particles in CsA-treated cells (Figure 6A, B). Moreover, neutralizing antibodies directed against IFNλ1, IFNλ2 and IFNλ3 or against the less induced IFNβ were applied (Figure 6B). Neutralization of IFNβ had no significant impact on MERS-CoV replication after CsA treatment, whereas application of anti-IFNλ1/2/3 treatment significantly increased MERS-CoV viral titers by 1.05 $\log_{10}$ level (Figure 6B). These data indicate that the antiviral effects of CsA were at least partially mediated by an IRF1-IFNλ signaling axis, and independent of type-I-IFN.

CsA-treatment upregulates IFNλ and leads to reduced MERS-CoV replication and lung pathology in vivo

To validate the antiviral efficacy of CsA against MERS-CoV *in vivo*, we used our recently established MERS-CoV infection mouse model that is based on the intratracheal delivery of the human DPP4 receptor to lung epithelial cells via adenoviral transduction, leading to severe MERS-CoV infection that presents as necrotizing interstitial pneumonia [22]. We treated mice daily via oral intake of either DMSO or CsA, starting 2 days before mock or MERS-CoV infection. Oral CsA application resulted in CsA serum levels of 202 to 356 ng/ml (mean 270 ±17 ng/ml), a

concentration that compares to levels reached in patients under CsA treatment (Supplement Figure E5, 34, 35). Accordingly, CsA treatment significantly induced release of IFNλ in the bronchoalveolar lavage fluid (Figure 7A). *IFNL* induction was significantly elevated in the CsA treatment group compared to DMSO-treated mice at day 7 post MERS-CoV infection (Figure 7B). Oral application of CsA significantly reduced viral titers (3.45 ±0.15 versus 2.1 ±0.36 $TCID_{50}$/ml in the DMSO versus CsA group) at day 7 post MERS-CoV infection (Figure 7C). CsA treatment did not alter adenoviral transduction efficiency (Supplemental Fig. E6). Of note, expression levels of *IFNL* inversely correlated with MERS-CoV load in lung homogenates at day 7 pi (Figure 7D). A significant reduction in viral titers and a significant correlation between *IFNL* induction and MERS-CoV inhibition could also be demonstrated at day 4 pi (Supplement Fig. E7). Expression of the *SCNN1B* gene (ENaCβ) as a marker of epithelial integrity was improved in lung homogenates of MERS-CoV-infected mice treated with CsA (Figure 7E). While extensive edema formation was present in a substantial portion of MERS-CoV-infected mice, it was absent in the CsA-treated group (Supplement Fig. E8). Importantly, the percentage of lung areas showing histopathological alterations due to MERS-CoV infection was significantly decreased by CsA treatment at day 7 post infection (Figure 7F). Collectively, we demonstrate that oral application of CsA induced IFNλ in the lungs of mice and exerted potent antiviral activity *in vivo*.

Discussion

With the appearance of SARS-CoV in 2002, MERS-CoV in 2012 and recently SARS-CoV-2, three species of the family *Coronaviridae* have revealed the ability to be efficiently transmitted from human-to-human and to provoke serious disease with high mortality rates. Both SARS-CoV and MERS-CoV are listed on the WHO blueprint list of priority diseases, and the zoonotic CoV reservoir strains are generally considered and have now been proven to be a source for emerging pandemic viruses.

As no specific treatment is approved for MERS-CoV or SARS-CoV(-2), current treatment strategies are supportive [29, 30]. Treatments including recombinant type-I-IFN and antivirals (e.g. Lopinavir/Ritonavir) have been applied off-label to treat MERS-CoV and yielded only moderate efficacy with controversial results in retrospective studies, and data from prospective studies or randomized controlled trials are lacking [29, 31–33]. Due to its receptor specificity to the human DPP4, only few animal models to study MERS-CoV pathogenesis and MERS-CoV-directed antiviral compounds have been accessible to date. For this study, MERS-CoV infection in the mouse was facilitated via intratracheal delivery of a human DPP4-encoding adenovirus, that might cause low-level inflammation itself and inhomogeneous receptor distribution within the lung, present for a limited time frame. However, even if this model might not fully recapitulate the native cellular distribution or density of the receptor as seen in the human lung, high transduction efficiencies (≥ 95%, data not shown) allow efficient viral spread in the upper and lower respiratory airways with quick progression to severe lung injury [22] and with moderate changes in morbidity [34]. Thus, model-specific neurotropism as seen in some of the

transgenic hDPP4 mice [35] or the necessity to adapt virus isolates via multiple passages, which might potentially affect its susceptibility to interventional strategies, are circumvented. While prior exposure to adenovirus evokes moderate histological changes including perivascular and bronchiolar lymphocytic infiltration (data not shown), MERS-CoV infection led to a clearly distinguishable granulocytic, necrotizing interstitial pneumonia with alveolar edema formation as described previously [22].

CsA has been implicated as inhibitor of a broad spectrum of virus families, including diverse CoV [14, 36–41]. However, studies on efficacy of CsA against CoV infection relied on results in liver and kidney cell lines [14–16], while results from primary lung epithelial target cells were lacking. Recently, CsA was demonstrated to restrict MERS-CoV *ex vivo* [13]. Still, insights on mechanistic details and on the question if CsA application would affect MERS-CoV infection *in vivo* remained elusive.

We now demonstrate that CsA application blocks MERS-CoV both at mRNA level and the amount of infectious viral particles released and significantly improves epithelial barrier integrity after MERS-CoV infection. Using different inhibitors known to block CsA-targeted pathways, we reveal that the CsA-induced blockade of MERS-CoV RNA synthesis can neither be reproduced by inhibition of known CsA-targeted MAP kinases nor by blockade of NFAT activation. Of note, ALV, which blocks CypA PPIase activity efficiently, but affects NFAT-dependent pathways only at very high concentrations [42], diminished MERS-CoV RNA accumulation as efficiently as CsA, suggesting that CypA plays a pivotal role in these processes. In fact, we revealed a previously unknown activation of genes involved in innate immune responses and in limitation of virus replication upon administration of CsA to lung epithelial cells.

Moreover, we demonstrate that inhibition of CypA via CsA or ALV, which both potently block the CypA PPIase activity at the used concentrations [42], results in a pronounced upregulation of type-III-IFN on both mRNA and protein level, which was mediated via IRF1 and was accompanied by expression of antiviral ISGs. Among those, especially IFIT1 (Interferon-induced protein with tetratricopeptide repeats 1), has been reported to influence the pathogenesis of MERS-CoV, highlighting the relevance of our findings [43].

Of note, type-III-IFNs have recently emerged as key antiviral players in the innate immune response to viral infections at mucosal and epithelial surfaces [44–47]. They efficiently restrict different respiratory viruses, and act e.g. by limiting spread from the upper to the lower airways [44, 46–48]. As opposed to type-I-IFN, type-III-IFN do not trigger detrimental immune responses that contribute to immunopathology in influenza infection [23, 25, 44, 49]. This might prove to be pivotal in the context of CsA-dependent stimulation of IFNλ during CoV, as severe human CoV infections, like MERS-CoV and– while data are still limited – also SARS-CoV-2, are characterized by an immunopathology with a strong cytokine induction [5, 50, 51].

In addition to defining a novel pro-inflammatory, antiviral expression profile induced by CsA on lung epithelial cells, this study also demonstrated for the first time that oral application of CsA reduces viral load in an *in vivo* MERS-CoV infection model. CsA is a licensed drug in clinical use since the 1980s. While prolonged treatment (over weeks and months) with CsA can induce side effects (e.g. nephrotoxicity; 48), we here applied a short-interval oral intake of CsA during acute infection. Our results demonstrate that *in vivo*, oral application over 6 days results in drug serum levels efficiently inhibiting lung viral infection and pneumonia

progression, highlighting CsA as a promising drug to be re-purposed for treatment of MERS-CoV.

Notably, our *in vitro* studies also revealed that neutralization of type-III-IFNs did not completely reverse the MERS-CoV-restrictive effect of CsA. We therefore suggest that CsA affects MERS-CoV at multiple steps during viral replication. In fact, we show that CsA acts on MERS-CoV propagation via inhibition of JNK, which is another downstream target of CsA [19, 53]. JNK inhibition has no impact on MERS-CoV RNA accumulation but strongly reduces the amount of released infectious virions. While the exact underlying molecular mechanisms remain to be defined, this finding demonstrated that CsA likely exerts additive effects to restrict MERS-CoV replication. While application of recombinant IFNs are approved to treat virus infections and malignancies, severe side effects have been related to systemic IFN application [54]. CsA repurposing for treatment of (MERS-) CoV infection might therefore come with several advantages over IFN treatment, such as additional antiviral effects beyond those mediated by IFNλ alone, a favorable side effect profile upon short-term use, a beneficial effect regarding an overshooting immune response characterizing CoV disease [55, 56] and proven oral availability (64, 65). CsA therefore represents a promising therapeutic option to combat human CoV infections, potentially extending over MERS-CoV to the current pandemic SARS-CoV-2 strain and future CoV threats.

Acknowledgements

Work with live MERS-CoV was performed in the BSL-4 facility of the Philipps University, Marburg, Germany. We thank Julia Spengler, Larissa Hamann, Stefanie Jarmer, Dirk Becker and Marc Ringel for excellent technical and experimental assistance. We thank Ralf Bartenschlager for providing Alisporivir.

Funding

This work was supported by the German Research Foundation (KFO309 P2/P8; Project ID: 284237345; SFB-TR84 B2, Project ID: 114933180; SFB1021 C05, Project ID: 197785619), by the German Center for Lung Research (DZL), by the German Center for Infection Research (DZIF) and the Cardio-Pulmonary Institute (CPI), EXC 2026, Project ID: 390649896.

References

1. Zaki AM, van Boheemen S, Bestebroer TM, Osterhaus ADME, Fouchier RAM. Isolation of a Novel Coronavirus from a Man with Pneumonia in Saudi Arabia. *N. Engl. J. Med.* [Internet] 2012 [cited 2019 Jan 9]; 367: 1814–1820Available from: http://www.ncbi.nlm.nih.gov/pubmed/23075143.

2. WHO. Middle East respiratory syndrome coronavirus (MERS-CoV) [Internet]. 2018 [cited 2019 Jan 10].Available from: https://www.who.int/en/news-room/fact-sheets/detail/middle-east-respiratory-syndrome-coronavirus-(mers-cov).

3. Raj VS, Mou H, Smits SL, Dekkers DHW, Müller MA, Dijkman R, Muth D, Demmers JAA, Zaki A, Fouchier RAM, Thiel V, Drosten C, Rottier PJM, Osterhaus ADME, Bosch BJ, Haagmans BL. Dipeptidyl peptidase 4 is a functional receptor for the emerging human coronavirus-EMC. *Nature* [Internet] 2013 [cited 2019 Jan 10]; 495: 251–254Available from: http://www.ncbi.nlm.nih.gov/pubmed/23486063.

4. Ng DL, Al Hosani F, Keating MK, Gerber SI, Jones TL, Metcalfe MG, Tong S, Tao Y, Alami NN, Haynes LM, Mutei MA, Abdel-Wareth L, Uyeki TM, Swerdlow DL, Barakat M, Zaki SR. Clinicopathologic, Immunohistochemical, and Ultrastructural Findings of a Fatal Case of Middle East Respiratory Syndrome Coronavirus Infection in the United Arab Emirates, April 2014. *Am. J. Pathol.* [Internet] Elsevier; 2016 [cited 2019 Jan 9]; 186: 652–658Available from: https://linkinghub.elsevier.com/retrieve/pii/S0002944015006471.

5. Alsaad KO, Hajeer AH, Al Balwi M, Al Moaiqel M, Al Oudah N, Al Ajlan A, AlJohani S, Alsolamy S, Gmati GE, Balkhy H, Al-Jahdali HH, Baharoon SA,

Arabi YM. Histopathology of Middle East respiratory syndrome coronovirus (MERS-CoV) infection - clinicopathological and ultrastructural study. *Histopathology* [Internet] 2018 [cited 2019 Jan 9]; 72: 516–524Available from: http://www.ncbi.nlm.nih.gov/pubmed/28858401.

6. Arabi YM, Balkhy HH, Hayden FG, Bouchama A, Luke T, Baillie JK, Al-Omari A, Hajeer AH, Senga M, Denison MR, Nguyen-Van-Tam JS, Shindo N, Bermingham A, Chappell JD, Van Kerkhove MD, Fowler RA. Middle East Respiratory Syndrome. *N. Engl. J. Med.* [Internet] Massachusetts Medical Society; 2017 [cited 2019 Jan 10]; 376: 584–594Available from: http://www.nejm.org/doi/10.1056/NEJMsr1408795.

7. Chan JF-W, Yao Y, Yeung M-L, Deng W, Bao L, Jia L, Li F, Xiao C, Gao H, Yu P, Cai J-P, Chu H, Zhou J, Chen H, Qin C, Yuen K-Y. Treatment With Lopinavir/Ritonavir or Interferon-β1b Improves Outcome of MERS-CoV Infection in a Nonhuman Primate Model of Common Marmoset. *J. Infect. Dis.* [Internet] 2015 [cited 2019 Jan 10]; 212: 1904–1913Available from: http://www.ncbi.nlm.nih.gov/pubmed/26198719.

8. Falzarano D, de Wit E, Rasmussen AL, Feldmann F, Okumura A, Scott DP, Brining D, Bushmaker T, Martellaro C, Baseler L, Benecke AG, Katze MG, Munster VJ, Feldmann H. Treatment with interferon-α2b and ribavirin improves outcome in MERS-CoV–infected rhesus macaques. *Nat. Med.* [Internet] Nature Research; 2013 [cited 2016 Oct 18]; 19: 1313–1317Available from: http://www.nature.com/doifinder/10.1038/nm.3362.

9. Falzarano D, de Wit E, Martellaro C, Callison J, Munster VJ, Feldmann H. Inhibition of novel β coronavirus replication by a combination of interferon-α2b

and ribavirin. *Sci. Rep.* [Internet] Nature Publishing Group; 2013 [cited 2019 Jan 10]; 3: 1686Available from: http://www.nature.com/articles/srep01686.

10. Omrani AS, Saad MM, Baig K, Bahloul A, Abdul-Matin M, Alaidaroos AY, Almakhlafi GA, Albarrak MM, Memish ZA, Albarrak AM. Ribavirin and interferon alfa-2a for severe Middle East respiratory syndrome coronavirus infection: a retrospective cohort study. *Lancet Infect. Dis.* [Internet] 2014 [cited 2019 Jan 10]; 14: 1090–1095Available from: http://www.ncbi.nlm.nih.gov/pubmed/25278221.

11. Al-Tawfiq JA, Momattin H, Dib J, Memish ZA. Ribavirin and interferon therapy in patients infected with the Middle East respiratory syndrome coronavirus: an observational study. *Int. J. Infect. Dis.* [Internet] 2014 [cited 2019 Jan 10]; 20: 42–46Available from: http://www.ncbi.nlm.nih.gov/pubmed/24406736.

12. Shalhoub S, Farahat F, Al-Jiffri A, Simhairi R, Shamma O, Siddiqi N, Mushtaq A. IFN-α2a or IFN-β1a in combination with ribavirin to treat Middle East respiratory syndrome coronavirus pneumonia: a retrospective study. *J. Antimicrob. Chemother.* [Internet] 2015 [cited 2019 Jan 10]; 70: 2129–2132Available from: http://www.ncbi.nlm.nih.gov/pubmed/25900158.

13. Li HS, Kuok DIT, Cheung MC, Ng MMT, Ng KC, Hui KPY, Peiris JSM, Chan MCW, Nicholls JM. Effect of interferon alpha and cyclosporine treatment separately and in combination on Middle East Respiratory Syndrome Coronavirus (MERS-CoV) replication in a human in-vitro and ex-vivo culture model. *Antiviral Res.* [Internet] 2018 [cited 2019 Jan 10]; 155: 89–96Available from: http://www.ncbi.nlm.nih.gov/pubmed/29772254.

14. de Wilde AH, Zevenhoven-Dobbe JC, van der Meer Y, Thiel V, Narayanan K, Makino S, Snijder EJ, van Hemert MJ. Cyclosporin A inhibits the replication of diverse coronaviruses. *J. Gen. Virol.* [Internet] 2011 [cited 2019 Jan 10]; 92: 2542–2548Available from: http://www.ncbi.nlm.nih.gov/pubmed/21752960.

15. Carbajo-Lozoya J, Ma-Lauer Y, Malešević M, Theuerkorn M, Kahlert V, Prell E, von Brunn B, Muth D, Baumert TF, Drosten C, Fischer G, von Brunn A. Human coronavirus NL63 replication is cyclophilin A-dependent and inhibited by non-immunosuppressive cyclosporine A-derivatives including Alisporivir. *Virus Res.* [Internet] Elsevier; 2014 [cited 2015 Dec 6]; 184: 44–53Available from: https://www.sciencedirect.com/science/article/abs/pii/S016817021400063X.

16. de Wilde AH, Raj VS, Oudshoorn D, Bestebroer TM, van Nieuwkoop S, Limpens RWAL, Posthuma CC, van der Meer Y, Barcena M, Haagmans BL, Snijder EJ, van den Hoogen BG. MERS-coronavirus replication induces severe in vitro cytopathology and is strongly inhibited by cyclosporin A or interferon-treatment. *J. Gen. Virol.* [Internet] 2013 [cited 2019 Jan 10]; 94: 1749–1760Available from: http://www.ncbi.nlm.nih.gov/pubmed/23620378.

17. Schiene-Fischer C. Multidomain Peptidyl Prolyl cis/trans Isomerases. *Biochim. Biophys. Acta - Gen. Subj.* [Internet] 2015 [cited 2019 Jan 10]; 1850: 2005–2016Available from: http://www.ncbi.nlm.nih.gov/pubmed/25445709.

18. Banerjee S, Narayanan K, Mizutani T, Makino S. Murine coronavirus replication-induced p38 mitogen-activated protein kinase activation promotes interleukin-6 production and virus replication in cultured cells. *J. Virol.* [Internet] 2002 [cited 2015 Feb 9]; 76: 5937–5948Available from: http://www.pubmedcentral.nih.gov/articlerender.fcgi?artid=136219&tool=pmcen

trez&rendertype=abstract.

19. Sugano N, Ito K, Murai S. Cyclosporin A inhibits collagenase gene expression via AP-1 and JNK suppression in human gingival fibroblasts. *J. Periodontal Res.* [Internet] John Wiley & Sons, Ltd (10.1111); 2010 [cited 2019 Jan 29]; 33: 448–452Available from: http://doi.wiley.com/10.1111/j.1600-0765.1998.tb02343.x.

20. Matsuda S, Moriguchi T, Koyasu S, Nishida E. T lymphocyte activation signals for interleukin-2 production involve activation of MKK6-p38 and MKK7-SAPK/JNK signaling pathways sensitive to cyclosporin A. *J. Biol. Chem.* [Internet] American Society for Biochemistry and Molecular Biology; 1998 [cited 2019 Jan 29]; 273: 12378–12382Available from: http://www.ncbi.nlm.nih.gov/pubmed/9575191.

21. Volz A, Kupke A, Song F, Jany S, Fux R, Shams-Eldin H, Schmidt J, Becker C, Eickmann M, Becker S, Sutter G. Protective Efficacy of Recombinant Modified Vaccinia Virus Ankara Delivering Middle East Respiratory Syndrome Coronavirus Spike Glycoprotein. Perlman S, editor. *J. Virol.* [Internet] 2015 [cited 2019 Jan 10]; 89: 8651–8656Available from: http://www.ncbi.nlm.nih.gov/pubmed/26018172.

22. Dietert K, Gutbier B, Wienhold SM, Reppe K, Jiang X, Yao L, Chaput C, Naujoks J, Brack M, Kupke A, Peteranderl C, Becker S, von Lachner C, Baal N, Slevogt H, Hocke AC, Witzenrath M, Opitz B, Herold S, Hackstein H, Sander LE, Suttorp N, Gruber AD. Spectrum of pathogen- and model-specific histopathologies in mouse models of acute pneumonia. Jeyaseelan S, editor. *PLoS One* [Internet] 2017 [cited 2019 Jan 10]; 12: e0188251Available from:

http://www.ncbi.nlm.nih.gov/pubmed/29155867.

23. Högner K, Wolff T, Pleschka S, Plog S, Gruber AD, Kalinke U, Walmrath H-D, Bodner J, Gattenlöhner S, Lewe-Schlosser P, Matrosovich M, Seeger W, Lohmeyer J, Herold S. Macrophage-expressed IFN-β contributes to apoptotic alveolar epithelial cell injury in severe influenza virus pneumonia. *PLoS Pathog.* [Internet] 2013 [cited 2014 Sep 19]; 9: e1003188Available from: http://www.pubmedcentral.nih.gov/articlerender.fcgi?artid=3585175&tool=pmcentrez&rendertype=abstract.

24. Malczyk AH, Kupke A, Prüfer S, Scheuplein VA, Hutzler S, Kreuz D, Beissert T, Bauer S, Hubich-Rau S, Tondera C, Eldin HS, Schmidt J, Vergara-Alert J, Süzer Y, Seifried J, Hanschmann K-M, Kalinke U, Herold S, Sahin U, Cichutek K, Waibler Z, Eickmann M, Becker S, Mühlebach MD. A Highly Immunogenic and Protective Middle East Respiratory Syndrome Coronavirus Vaccine Based on a Recombinant Measles Virus Vaccine Platform. Perlman S, editor. *J. Virol.* [Internet] 2015 [cited 2019 Jul 19]; 89: 11654–11667Available from: http://www.ncbi.nlm.nih.gov/pubmed/26355094.

25. Peteranderl C, Morales-Nebreda L, Selvakumar B, Lecuona E, Vadász I, Morty RE, Schmoldt C, Bespalowa J, Wolff T, Pleschka S, Mayer K, Gattenloehner S, Fink L, Lohmeyer J, Seeger W, Sznajder JI, Mutlu GM, Budinger GRS, Herold S, Jain S, Short K, Kroeze E, Fouchier R, Kuiken T, Kuiken T, Taubenberger J, Herold S, Matthay M, Ware L, Zimmerman G, et al. Macrophage-epithelial paracrine crosstalk inhibits lung edema clearance during influenza infection. *J. Clin. Invest.* [Internet] American Society for Clinical Investigation; 2016 [cited 2016 Sep 11]; 126: 1566–1580Available from:

https://www.jci.org/articles/view/83931.

26. Odendall C, Kagan JC. The unique regulation and functions of type III interferons in antiviral immunity. *Curr. Opin. Virol.* [Internet] 2015 [cited 2016 Sep 11]; 12: 47–52Available from: http://www.ncbi.nlm.nih.gov/pubmed/25771505.

27. Karamehic J, Asceric M, Tulumovic T, Uzeirbegovic M, Hadzibegic N. [Serum cyclosporine levels in patients after kidney transplantation]. *Med Arh* [Internet] Zavod za farmakologiju i toksikologiju sa klinickom farmakologijom, Medicinski fakultet Tuzla.; 1998; 52: 131–132Available from: http://www.ncbi.nlm.nih.gov/pubmed/9863315.

28. Narula AS, Murthy M, Patrulu K, Saxena VK. Routine Cyclosporine concentration - C2 level Monitoring. Is it helpful during the early post Transplant Period? *Med. journal, Armed Forces India* [Internet] 2004 [cited 2019 Jul 11]; 60: 326–328Available from: https://linkinghub.elsevier.com/retrieve/pii/S0377123704800030.

29. Zumla A, Chan JFW, Azhar EI, Hui DSC, Yuen K-Y. Coronaviruses — drug discovery and therapeutic options. *Nat. Rev. Drug Discov.* [Internet] Nature Publishing Group; 2016 [cited 2019 Jan 29]; 15: 327–347Available from: http://www.nature.com/articles/nrd.2015.37.

30. Guan W-J, Ni Z-Y, Hu Y, Liang W-H, Ou C-Q, He J-X, Liu L, Shan H, Lei C-L, Hui DSC, Du B, Li L-J, Zeng G, Yuen K-Y, Chen R-C, Tang C-L, Wang T, Chen P-Y, Xiang J, Li S-Y, Wang J-L, Liang Z-J, Peng Y-X, Wei L, Liu Y, Hu Y-H, Peng P, Wang J-M, Liu J-Y, Chen Z, et al. Clinical Characteristics of

Coronavirus Disease 2019 in China. *N. Engl. J. Med.* 2020; .

31. Sheahan TP, Sims AC, Graham RL, Menachery VD, Gralinski LE, Case JB, Leist SR, Pyrc K, Feng JY, Trantcheva I, Bannister R, Park Y, Babusis D, Clarke MO, Mackman RL, Spahn JE, Palmiotti CA, Siegel D, Ray AS, Cihlar T, Jordan R, Denison MR, Baric RS. Broad-spectrum antiviral GS-5734 inhibits both epidemic and zoonotic coronaviruses. *Sci. Transl. Med.* [Internet] 2017 [cited 2019 Feb 15]; 9: eaal3653Available from: http://www.ncbi.nlm.nih.gov/pubmed/28659436.

32. Arabi YM, Alothman A, Balkhy HH, Al-Dawood A, AlJohani S, Al Harbi S, Kojan S, Al Jeraisy M, Deeb AM, Assiri AM, Al-Hameed F, AlSaedi A, Mandourah Y, Almekhlafi GA, Sherbeeni NM, Elzein FE, Memon J, Taha Y, Almotairi A, Maghrabi KA, Qushmaq I, Al Bshabshe A, Kharaba A, Shalhoub S, Jose J, Fowler RA, Hayden FG, Hussein MA, And the MIRACLE trial group. Treatment of Middle East Respiratory Syndrome with a combination of lopinavir-ritonavir and interferon-β1b (MIRACLE trial): study protocol for a randomized controlled trial. *Trials* [Internet] 2018 [cited 2019 Jan 10]; 19: 81Available from: http://www.ncbi.nlm.nih.gov/pubmed/29382391.

33. Al-Tawfiq JA, Memish ZA. Update on therapeutic options for Middle East Respiratory Syndrome Coronavirus (MERS-CoV). *Expert Rev. Anti. Infect. Ther.* [Internet] 2017 [cited 2019 Jan 29]; 15: 269–275Available from: http://www.ncbi.nlm.nih.gov/pubmed/27937060.

34. Zhao J, Li K, Wohlford-Lenane C, Agnihothram SS, Fett C, Zhao J, Gale MJ, Baric RS, Enjuanes L, Gallagher T, McCray PB, Perlman S. Rapid generation of a mouse model for Middle East respiratory syndrome. *Proc. Natl. Acad. Sci.*

[Internet] National Academy of Sciences; 2014 [cited 2020 Mar 13]; 111: 4970–4975Available from: https://www.pnas.org/content/111/13/4970.

35. Agrawal AS, Garron T, Tao X, Peng B-H, Wakamiya M, Chan T-S, Couch RB, Tseng C-TK. Generation of a Transgenic Mouse Model of Middle East Respiratory Syndrome Coronavirus Infection and Disease. *J. Virol.* 2015; .

36. Ma C, Li F, Musharrafieh RG, Wang J. Discovery of cyclosporine A and its analogs as broad-spectrum anti-influenza drugs with a high in vitro genetic barrier of drug resistance. *Antiviral Res.* [Internet] 2016 [cited 2019 Feb 1]; 133: 62–72Available from: http://www.ncbi.nlm.nih.gov/pubmed/27478032.

37. Nkongolo S, Ni Y, Lempp FA, Kaufman C, Lindner T, Esser-Nobis K, Lohmann V, Mier W, Mehrle S, Urban S. Cyclosporin A inhibits hepatitis B and hepatitis D virus entry by cyclophilin-independent interference with the NTCP receptor. *J. Hepatol.* [Internet] Elsevier; 2014 [cited 2019 Feb 1]; 60: 723–731Available from: https://www.sciencedirect.com/science/article/abs/pii/S0168827813008246.

38. Nakagawa M, Sakamoto N, Tanabe Y, Koyama T, Itsui Y, Takeda Y, Chen C, Kakinuma S, Oooka S, Maekawa S, Enomoto N, Watanabe M. Suppression of Hepatitis C Virus Replication by Cyclosporin A Is Mediated by Blockade of Cyclophilins. *Gastroenterology* [Internet] W.B. Saunders; 2005 [cited 2019 Feb 1]; 129: 1031–1041Available from: https://www.sciencedirect.com/science/article/pii/S0016508505011923.

39. Karpas A, Lowdell M, Jacobson SK, Hill F. Inhibition of human immunodeficiency virus and growth of infected T cells by the

immunosuppressive drugs cyclosporin A and FK 506. *Proc. Natl. Acad. Sci. U. S. A.* [Internet] National Academy of Sciences; 1992 [cited 2019 Feb 1]; 89: 8351–8355Available from: http://www.ncbi.nlm.nih.gov/pubmed/1381509.

40. Zhang W, Shi Y, Qi J, Gao F, Li Q, Fan Z, Yan J, Gao GF. Molecular basis of the receptor binding specificity switch of the hemagglutinins from both the 1918 and 2009 pandemic influenza A viruses by a D225G substitution. *J. Virol.* [Internet] 2013 [cited 2014 Aug 22]; 87: 5949–5958Available from: http://www.pubmedcentral.nih.gov/articlerender.fcgi?artid=3648181&tool=pmcentrez&rendertype=abstract.

41. Shen Z, He H, Wu Y, Li J. Cyclosporin A Inhibits Rotavirus Replication and Restores Interferon-Beta Signaling Pathway In Vitro and In Vivo. Ho W, editor. *PLoS One* [Internet] Public Library of Science; 2013 [cited 2019 Jan 17]; 8: e71815Available from: https://dx.plos.org/10.1371/journal.pone.0071815.

42. Gallay PA. Cyclophilin inhibitors: a novel class of promising host-targeting anti-HCV agents. *Immunol. Res.* [Internet] Springer-Verlag; 2012 [cited 2019 Feb 15]; 52: 200–210Available from: http://link.springer.com/10.1007/s12026-011-8263-5.

43. Menachery VD, Gralinski LE, Mitchell HD, Dinnon KH, Leist SR, Yount BL, Graham RL, McAnarney ET, Stratton KG, Cockrell AS, Debbink K, Sims AC, Waters KM, Baric RS, Waters KM, Baric RS. Middle East Respiratory Syndrome Coronavirus Nonstructural Protein 16 Is Necessary for Interferon Resistance and Viral Pathogenesis. *mSphere* [Internet] American Society for Microbiology (ASM); 2017 [cited 2019 Jan 18]; 2Available from: http://www.ncbi.nlm.nih.gov/pubmed/29152578.

44. Davidson S, McCabe TM, Crotta S, Gad HH, Hessel EM, Beinke S, Hartmann R, Wack A. IFNλ is a potent anti-influenza therapeutic without the inflammatory side effects of IFNα treatment. *EMBO Mol. Med.* [Internet] Wiley-Blackwell; 2016 [cited 2019 Jan 29]; 8: 1099–1112Available from: http://www.ncbi.nlm.nih.gov/pubmed/27520969.

45. Lazear HM, Nice TJ, Diamond MS. Interferon-λ: Immune Functions at Barrier Surfaces and Beyond. *Immunity* [Internet] NIH Public Access; 2015 [cited 2019 Jan 29]; 43: 15–28Available from: http://www.ncbi.nlm.nih.gov/pubmed/26200010.

46. Klinkhammer J, Schnepf D, Ye L, Schwaderlapp M, Gad HH, Hartmann R, Garcin D, Mahlakõiv T, Staeheli P. IFN-λ prevents influenza virus spread from the upper airways to the lungs and limits virus transmission. *Elife* [Internet] eLife Sciences Publications, Ltd; 2018 [cited 2019 Jan 29]; 7Available from: http://www.ncbi.nlm.nih.gov/pubmed/29651984.

47. Hamming OJ, Terczyńska-Dyla E, Vieyres G, Dijkman R, Jørgensen SE, Akhtar H, Siupka P, Pietschmann T, Thiel V, Hartmann R. Interferon lambda 4 signals via the IFNλ receptor to regulate antiviral activity against HCV and coronaviruses. *EMBO J.* [Internet] European Molecular Biology Organization; 2013 [cited 2019 Jan 17]; 32: 3055–3065Available from: http://www.ncbi.nlm.nih.gov/pubmed/24169568.

48. Baños-Lara MDR, Harvey L, Mendoza A, Simms D, Chouljenko VN, Wakamatsu N, Kousoulas KG, Guerrero-Plata A. Impact and regulation of lambda interferon response in human metapneumovirus infection. *J. Virol.* [Internet] American Society for Microbiology Journals; 2015 [cited 2019 Feb

15]; 89: 730–742Available from: http://www.ncbi.nlm.nih.gov/pubmed/25355870.

49. Galani IE, Triantafyllia V, Eleminiadou E-E, Koltsida O, Stavropoulos A, Manioudaki M, Thanos D, Doyle SE, Kotenko S V., Thanopoulou K, Andreakos E. Interferon-λ Mediates Non-redundant Front-Line Antiviral Protection against Influenza Virus Infection without Compromising Host Fitness. *Immunity* [Internet] 2017 [cited 2019 Feb 15]; 46: 875-890.e6Available from: http://www.ncbi.nlm.nih.gov/pubmed/28514692.

50. Channappanavar R, Perlman S. Pathogenic human coronavirus infections: causes and consequences of cytokine storm and immunopathology. *Semin. Immunopathol.* [Internet] 2017 [cited 2019 Jan 29]; 39: 529–539Available from: http://www.ncbi.nlm.nih.gov/pubmed/28466096.

51. Qin C, Zhou L, Hu Z, Zhang S, Yang S, Tao Y, Xie C, Ma K, Shang K, Wang W, Tian D-S. Dysregulation of immune response in patients with COVID-19 in Wuhan, China. *Clin Infect Dis* 2020; Epub ahead: pii: ciaa248.

52. Watts R, Clunie G, Hall F. Rheumatology [Internet]. Oxford University Press; 2009 [cited 2019 Feb 1].Available from: https://books.google.de/books?id=1m_59s7Tt3UC&pg=PA558&redir_esc=y#v=onepage&q&f=false.

53. Matsuda S, Moriguchi T, Koyasu S, Nishida E. T Lymphocyte Activation Signals for Interleukin-2 Production Involve Activation of MKK6-p38 and MKK7-SAPK/JNK Signaling Pathways Sensitive to Cyclosporin A. *J. Biol. Chem.* [Internet] American Society for Biochemistry and Molecular Biology; 1998 [cited

2015 Feb 9]; 273: 12378–12382Available from: http://www.ncbi.nlm.nih.gov/pubmed/9575191.

54. Lasfar A, Zloza A, Cohen-Solal KA. IFN-lambda therapy: current status and future perspectives. *Drug Discov Today* [Internet] Department of Pharmacology and Toxicology, Ernest Mario School of Pharmacy, Rutgers, State University of New Jersey, Piscataway, NJ, USA; Rutgers Cancer Institute of New Jersey, New Brunswick, NJ, USA. Electronic address: ahmed.lasfar@pharmacy.rutgers.edu; 2016; 21: 167–171Available from: http://www.ncbi.nlm.nih.gov/pubmed/26552337.

55. DeDiego ML, Nieto-Torres JL, Regla-Nava JA, Jimenez-Guardeno JM, Fernandez-Delgado R, Fett C, Castano-Rodriguez C, Perlman S, Enjuanes L. Inhibition of NF- B-Mediated Inflammation in Severe Acute Respiratory Syndrome Coronavirus-Infected Mice Increases Survival. *J. Virol.* 2014; .

56. Li G, Fan Y, Lai Y, Han T, Li Z, Zhou P, Pan P, Wang W, Hu D, Liu X, Zhang Q, Wu J. Coronavirus infections and immune responses. J. Med. Virol. 2020.

57. Giordanetto F, Kihlberg J. Macrocyclic Drugs and Clinical Candidates: What Can Medicinal Chemists Learn from Their Properties? *J. Med. Chem.* [Internet] American Chemical Society; 2014 [cited 2019 Feb 19]; 57: 278–295Available from: http://pubs.acs.org/doi/10.1021/jm400887j.

58. Fellner RC, Terryah ST, Tarran R. Inhaled protein/peptide-based therapies for respiratory disease. *Mol. Cell. Pediatr.* [Internet] Springer; 2016 [cited 2019 Feb 19]; 3: 16Available from: http://www.ncbi.nlm.nih.gov/pubmed/27098663.

59. Sauerhering L, Müller H, Behner L, Elvert M, Fehling SK, Strecker T, Maisner

A. Variability of interferon-λ induction and antiviral activity in nipah virus infected differentiated human bronchial epithelial cells of two human donors. *J. Gen. Virol.* 2017.

Figure legends

Figure 1: Cyclosporin A (CsA) inhibits MERS-CoV replication and release in human airway epithelial cells and primary human alveolar epithelial cells (hAEC). Calu-3 and hAEC were infected with MERS-CoV using an MOI of 0.1, stimulated with DMSO or 10 µM Cyclosporin A (CsA), and analyzed at 24h pi. In (**A**), total RNA was isolated from cell lysates and viral RNA content was analyzed by qPCR. After normalization to actin, changes in RNA content in CsA-treated cells were normalized to RNA present in DMSO-treated control groups (set at 100%). In (**B**), virus titers were determined by $TCID_{50}$ method from cell-free culture supernatant and shown as $logTCID_{50}$/ml. In addition, (**C**) MERS-CoV-induced CPE and foci formation (marked by arrows) was documented in live cells by phase contrast microscopy at a magnification of 100x. (**D**) Apoptosis induction was quantified by Caspase 3/7 Glo® Assay in Calu-3. In (**E**), cell lysates were analyzed by western blot for expression of CFTR (168 kDa) and vinculin (120 kDa). Left panel shows representative western blots of n = 3 – 4 experiments. Right panel shows relative quantitation with mock samples set to 100%. (**F, G**) Calu-3 were grown on transwell filters and treated as above. Epithelial integrity was quantified by transepithelial resistance measurements (**F**) and vectorial water transport evaluated by FITC-Dextran quantification 48h pi (**G**). Bar graphs in (**A, B, D-G**) represent means ±SEM of n = 3 - 6 experiments. Statistical significance was analyzed by unpaired 2-tailed Student's t test (**A, B**) and one-way-ANOVA and Bonferroni's multiple comparisons test (**D-G**), where all groups were compared to each other. *P < 0.05; **P < 0.01; ***P < 0.005. Shown micrographs (**C**) are representative of n > 5 experiments.

Figure 2: Effect of CsA, ALV, and inhibition of CsA-dependent CnA/NFAT and MAPK pathways on MERS-CoV infection. Calu-3 (**A, C**) and hAEC (**B, D**) were infected with MERS-CoV using an MOI of 0.1. One hour after viral adsorption, cells were stimulated with either CsA (10 µM), its non-immunosuppressive derivate Alisporivir (ALV, 10 µM), Calcineurin (CnA) inhibitor (CIP, 20 µM), NFAT inhibitor (50 µM), JNK inhibitor (SP600125, 10 µM), p38 MAPK inhibitor (SB 203580, 10 µM) or DMSO as solvent control. In (**A, B**), virus titers were determined by $TCID_{50}$ method from cell-free culture supernatant and shown as log$TCID_{50}$/ml. In (**C, D**), total RNA was isolated from cell lysates at 24 h pi and viral RNA content was analyzed by qPCR. After normalization to actin, changes in RNA content in CsA-treated cells were normalized to RNA present in DMSO-treated control groups (set at 100%). Bar graphs represent means ± SEM of n = 6 - 8 experiments for DMSO and CsA groups and 3 - 5 experiments for ALV, CnA, NFAT, JNK and p38 inhibitors. Statistical significance was analyzed by one-way-ANOVA and Bonferroni's multiple comparisons test, where all groups were compared to each other. Statistical significances in comparison to DMSO control are indicated in the graph. *P < 0.05; **P < 0.01; ***P < 0.005; ns = not significant.

Figure 3: CsA treatment induces an antiviral response state in Calu-3 lung epithelial cells. Calu-3 cells were stimulated with 10 µM CsA or treated with DMSO as vehicle control. At 24 h post stimulation, total RNA was isolated and subjected to transcriptome analysis (see methods section). In (**A**), an over-representation analysis of GO biological processes was calculated using upregulated genes with a Log2FoldChange > 1. The 10 most significant biological processes are plotted in

order of gene ratio. The size of the dots represents the number of genes in the upregulated gene list associated with the GO term; the colors of the dots represent P-adjusted values. Individual genes are shown as heat map in (**B**) listing the top 50 regulated genes (up and down) and as volcano plot (**C**). Data represent two independent experiments.

Figure 4: CsA induces IFNλ mRNA and release. Calu-3 cells were stimulated with 10 µM CsA, followed by (**A**) total RNA isolation at 15, 18, 21, and 26 h after treatment. After cDNA synthesis, qPCR-analysis was performed for *IFNA*, *IFNB*, *IFNL1* and *IFNL2/3*. Fold change over DMSO-stimulated control was performed ($2^{-\Delta\Delta Ct}$) to visualize IFN-induction upon CsA stimulation. For quantification of released IFNλ (**B**), supernatants of CsA-stimulated Calu-3 cells were collected from 6 to 56 h after CsA treatment and IFNλ1/3 was determined by ELISA. (**C**) Expression of selected ISGs upon CsA treatment was analyzed at 18 h post CsA-treatment by qPCR-analysis and fold change over DMSO-stimulated control ($2^{-\Delta\Delta Ct}$). Bar graphs represent means ± SEM of n = 3 - 5 experiments in (**A, B**) and of n = 3 experiments in (**C**). Grey, dotted line in (**B**) represents the minimal detection limit of the ELISA as given by the manufacturer.

Figure 5: IRF1 mediates the CsA-induced expression of IFNλ. (**A**) Calu-3 cell lysates were collected 4 hours post treatment with 10µM CsA or DMSO control. Total RNA was isolated, and qPCRs for *IRF1*, *IRF3*, *IRF7*, and *IRF9* was performed. Data are presented as fold change over DMSO ($2^{-\Delta\Delta ct}$). (**B**) Expression of IRF1 in CsA or DMSO stimulated Calu-3 cells was analyzed by indirect immunofluorescence on

fixed and permeabilized cells (left panel). Nuclei were counterstained with DAPI. For quantification of IRF1 expression (right panel), the ratio of $IRF1^{positive}$ to $DAPI^{positive}$ cells were counted in at least 10 randomly chosen microscopic fields of 3 independent experiments. In (**C, D**), *IRF1* was silenced by siRNA-transfection experiments using oligofectamine. Scrambled siRNA transfection was used as control. At 4 h post transfection, Calu-3 cells were treated with 10 µM CsA. (**C**) Supernatants were collected 18 h after CsA treatment. *IFNL* mRNA was analyzed via qPCR. Data are shown as relative fold induction in comparison to non-siRNA treated cells (set to 100%). In (**D**) supernatants of siRNA-transfected and CsA stimulated cells were analyzed by ELISA. Data are shown as relative amount of IFNλ in comparison to non-siRNA treated cells (set to 100%). Bar graphs represent means ± SEM of n = 3 - 4 experiments for (**A**), n = 3 experiments for (**B, C**), and n = 4 experiments for (**D**). Statistical significance was calculated using unpaired 2-tailed Student's t test for (**B**) and one-way ANOVA and Bonferroni's multiple comparisons test comparing all groups to each other (**C, D**). *P < 0.05; **P < 0.01; ***P < 0.005; ns not significant.

Figure 6: Inhibition of the IRF1-IFNλ signaling axis partially prevents the CsA-induced effects on MERS-CoV replication. (**A**) *IRF1* was silenced by siRNA-transfection experiments using oligofectamine. Scrambled siRNA transfection was used as control. At 20 h post transfection, Calu-3 cells were infected with MERS-CoV at MOI 0.1 and after 1 h of viral adsorption cells were treated with 10 µM CsA or DMSO solvent control. 24 h pi, viral release was determined by $TCID_{50}$. In (**B**), Calu-3 cells were infected with MERS-CoV at MOI 0.1 and stimulated with CsA or DMSO

control as described before. In parallel, neutralizing antibodies targeting IFNβ or IFNλ1/2/3 were added simultaneously with CsA. 24 h pi viral release was determined by $TCID_{50}$. Bar graphs represent means ± SEM of n = 4 experiments in (**A**), and n = 6 - 7 experiments in (**B**). Statistical significance was calculated using one-way ANOVA and Bonferroni's multiple comparisons test, where all groups were compared to each other. Statistical significances in comparison to the oligofectamin-only treated group are indicated in the graph. *P < 0.05; **P < 0.01; ns not significant.

Figure 7: CsA-treatment upregulates IFNλ and reduces MERS-CoV replication *in vivo.*

(A) Mice were fed with CsA (50mg/kg/day) or DMSO as solvent control. After 6 days of daily oral application, levels of IFNλ were analyzed by ELISA from the bronchoalveolar lavage fluid. (**B-F**) Mice were intratracheally infected with an adenovirus construct encoding for human DPP4 and mCherry (Ad-hDPP4). Oral application of CsA (50mg/kg/day) or DMSO as solvent control was started at day 3 post transduction, while mice were infected with $1.5x10^5$ $TCID_{50}$/ml MERS-CoV via the intranasal route at day 5 post transduction. Mice were euthanized and lungs were isolated 7 days post MERS-CoV infection. Lung homogenate was used to quantify (**B**) relative *IFNL2/3* mRNA and (**C**) determine viral load by $TCID_{50}$. In (**D**) correlation between MERS-CoV titers and *IFNL2/3* mRNA expression levels was calculated using Pearson correlation efficient. In (**E**) relative amounts of *SCNNB1* (ENaCβ) RNA were determined via qPCR from lung homogenates of MERS-CoV-infected and DMSO- versus CsA-treated mice. In (**F**), lungs were fixed and processed for histological analysis. Lung areas characterized by interstitial inflammation typical for

MERS-CoV-induced pneumonia [22] were quantified after whole lung processing. Statistical significance was calculated using unpaired two-way student's t-test (**A, B, C, D, G**) with *P < 0.05.

Figure 8: CsA and ALV restrict MERS-CoV via induction of interferon lambda. Addition of cyclophilin inhibitors, including CsA or its non-immunosuppressive derivate ALV are known modulators of Cyclophilin A (CypA) and induce activation of the interferon regulatory transcription factor IRF1. Subsequently, transcription of type III interferon genes (*IFNL*) is upregulated and IFNλ is released both *in vitro* and *in vivo*. CsA further induces the expression of interferon stimulated genes (ISGs), likely by auto- and paracrine signaling via IFNλ. CsA-induced ISGs include molecules with a known antiviral effect, e.g. OAS1 or IFIT1, which in turn convey the restrictive effect of CsA on MERS-CoV replication.

List of abbreviations

(h)AEC	(human) alveolar epithelial cells
ALV	Alisporivir
CFTR	Cystic fibrosis transmembrane conductance regulator
CnA	Calcineurin
CsA	Cyclosporin A
CypA	Cyclophilin A
IFIT	Interferon-induced protein with tetratricopeptide repeats

IFN	Interferon
IRF	Interferon regulatory factor
ISG	Interferon-stimulated gene
JNK	c-Jun N-terminal kinase
MERS-CoV	Middle East respiratory syndrome coronavirus
MOI	Multiplicity of infection
NFAT	Nuclear factor of activated T-cells
pi	Post infection, time after infection
ps	Post stimulation
pt	Post transfection
PPIase	Peptidyl-prolyl cis-trans isomerase
SARS-CoV	Severe acute respiratory syndrome-related coronavirus
$TCID_{50}$	Tissue culture infection dose 50

Figure 1.

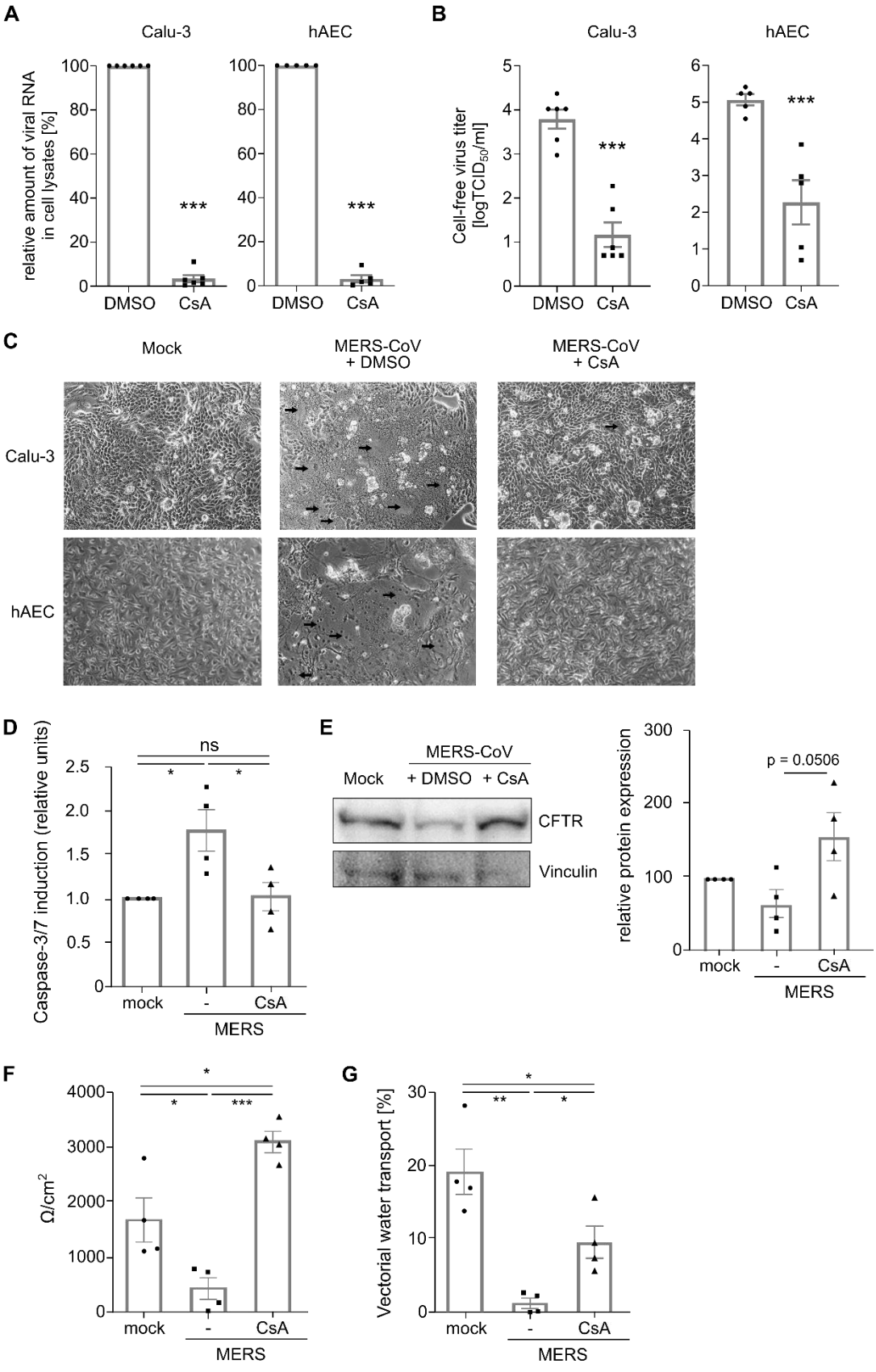
A
Calu-3
hAEC
relative amount of viral RNA in cell lysates [%]
100
80
60
40
20
0
***
DMSO
CsA
B
Calu-3
hAEC
Cell-free virus titer [logTCID50/ml]
5
4
3
2
1
0
6
***
DMSO
CsA
C
Mock
MERS-CoV + DMSO
MERS-CoV + CsA
Calu-3
hAEC
D
Caspase-3/7 induction (relative units)
ns
*
2.5
2.0
1.5
1.0
0.5
0
mock
-
CsA
MERS
E
MERS-CoV
Mock
+ DMSO
+ CsA
CFTR
Vinculin
relative protein expression
300
200
100
0
p = 0.0506
mock
-
CsA
MERS
F
Ω/cm2
4000
3000
2000
1000
0
*
***
mock
-
CsA
MERS
G
Vectorial water transport [%]
30
20
10
0
**
mock
-
CsA
MERS

Figure 2.

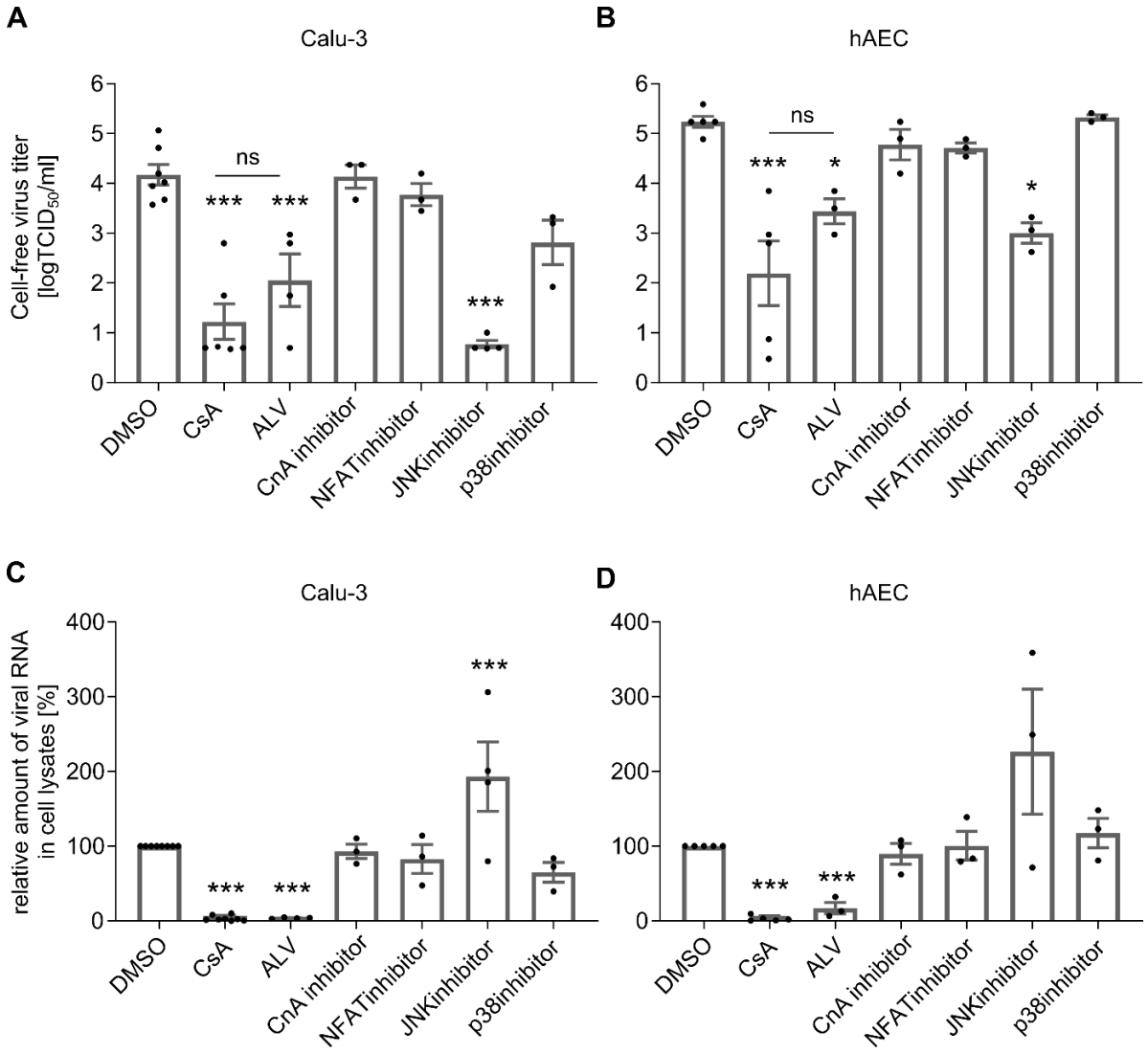
A
Calu-3
Cell-free virus titer [logTCID50/ml]
ns
***
***
***
DMSO
CsA
ALV
CnA inhibitor
NFATinhibitor
JNKinhibitor
p38inhibitor
B
hAEC
ns
***
*
*
C
Calu-3
relative amount of viral RNA in cell lysates [%]
***
***
***
D
hAEC
***
***

Figure 3.

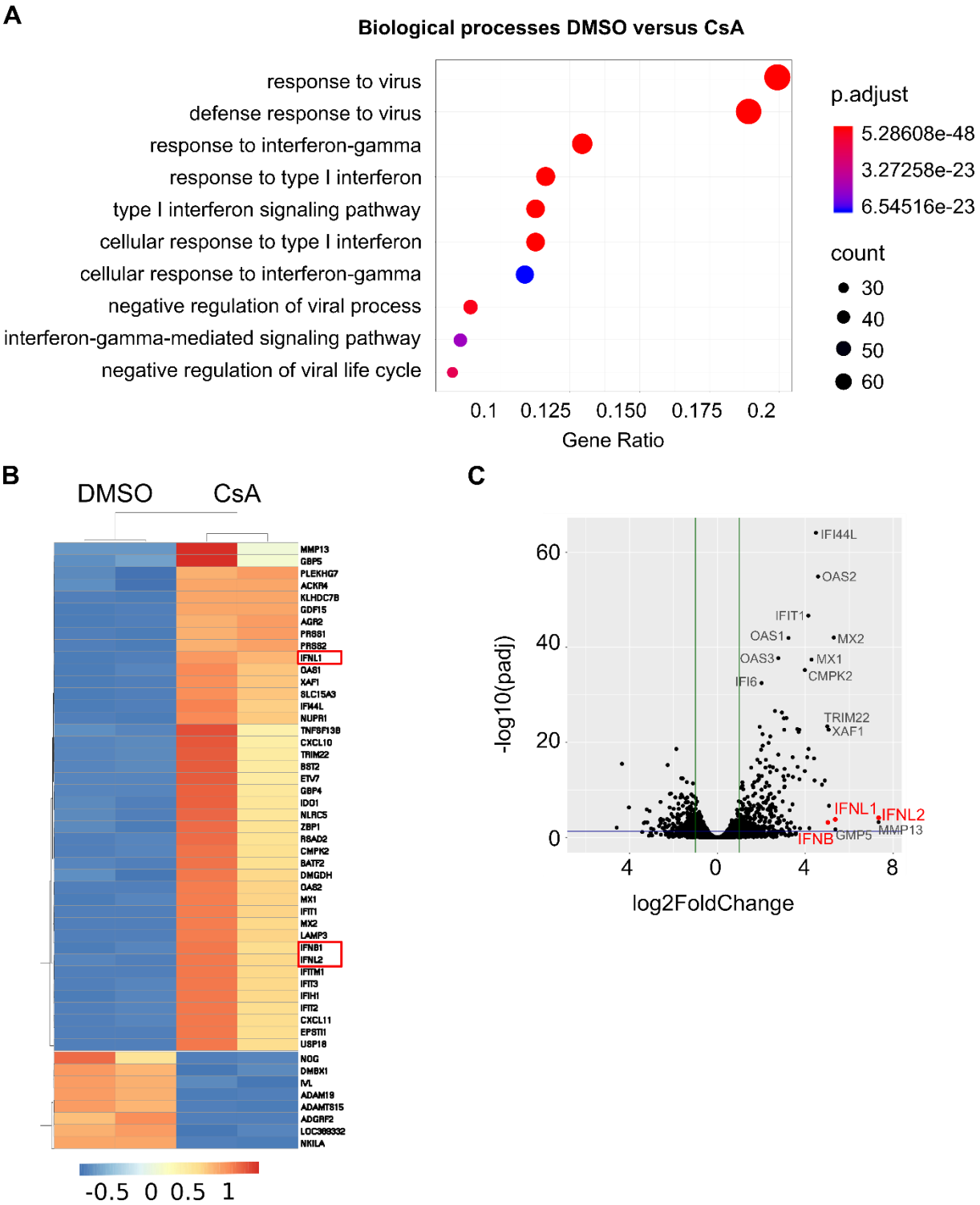
A
Biological processes DMSO versus CsA
response to virus
defense response to virus
response to interferon-gamma
response to type I interferon
type I interferon signaling pathway
cellular response to type I interferon
cellular response to interferon-gamma
negative regulation of viral process
interferon-gamma-mediated signaling pathway
negative regulation of viral life cycle
0.1
0.125
0.150
0.175
0.2
Gene Ratio
p.adjust
5.28608e-48
3.27258e-23
6.54516e-23
count
30
40
50
60
B
DMSO
CsA
MMP13
GBP5
PLEKHG7
ACKR4
KLHDC7B
GDF15
AGR2
PRSS1
PRSS2
IFNL1
OAS1
XAF1
SLC15A3
IFI44L
NUPR1
TNFSF13B
CXCL10
TRIM22
BST2
ETV7
GBP4
IDO1
NLRC5
ZBP1
RSAD2
CMPK2
BATF2
DMGDH
OAS2
MX1
IFIT1
MX2
LAMP3
IFNB1
IFNL2
IFITM1
IFIT3
IFIH1
IFIT2
CXCL11
EPSTI1
USP18
NOG
DMBX1
IVL
ADAM19
ADAMTS15
ADGRF2
LOC389332
NKILA
-0.5
0
0.5
1
C
-log10(padj)
60
40
20
0
IFI44L
OAS2
IFIT1
OAS1
MX2
OAS3
MX1
CMPK2
IFI6
TRIM22
XAF1
IFNL1
IFNL2
IFNB
GMP5
MMP13
4
0
4
8
log2FoldChange

Figure 4.

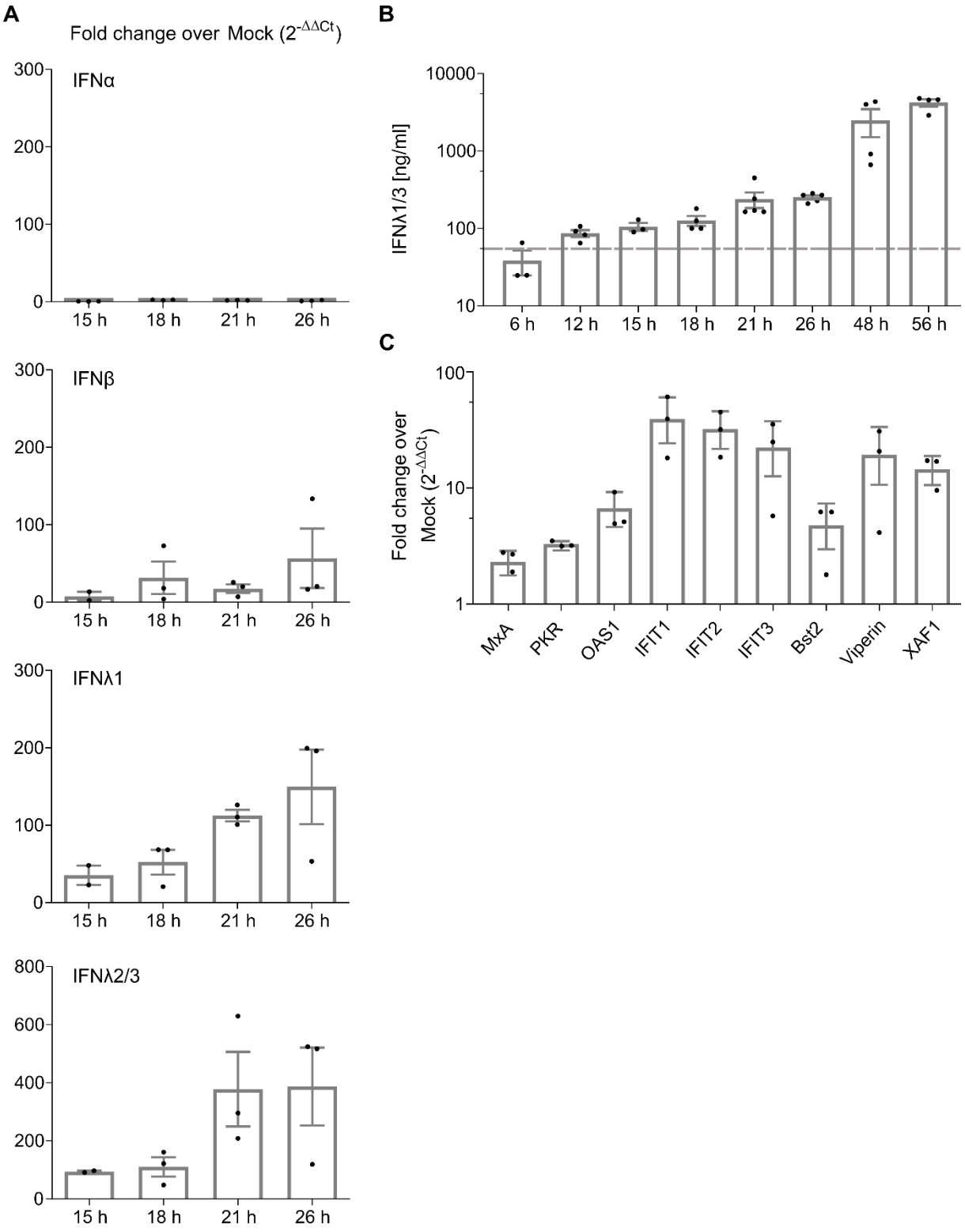
A
Fold change over Mock (2-ΔΔCt)
IFNα
IFNβ
IFNλ1
IFNλ2/3
15 h
18 h
21 h
26 h
B
IFNλ1/3 [ng/ml]
6 h
12 h
15 h
18 h
21 h
26 h
48 h
56 h
C
Fold change over Mock (2-ΔΔCt)
MxA
PKR
OAS1
IFIT1
IFIT2
IFIT3
Bst2
Viperin
XAF1

Figure 5.

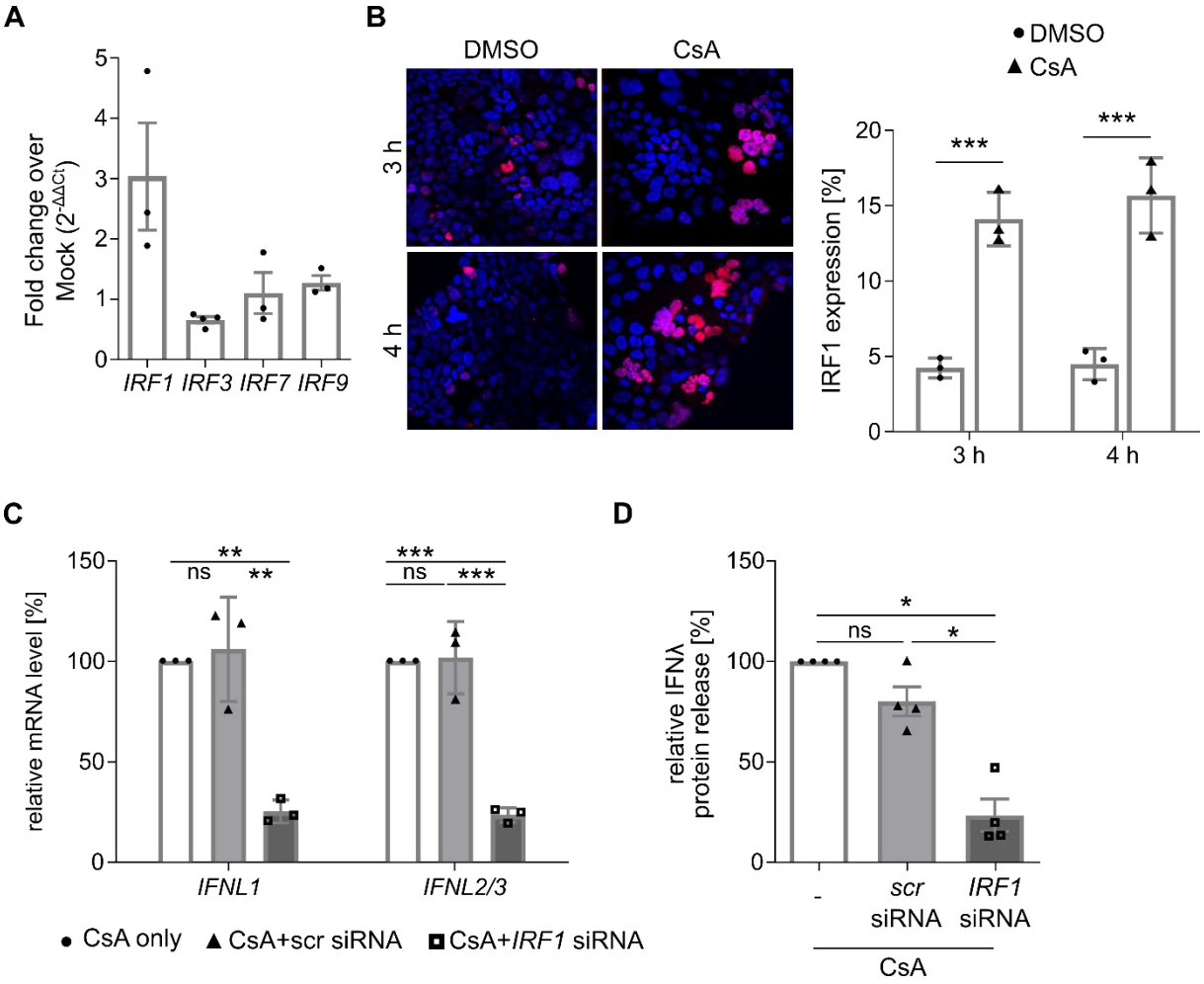
A
Fold change over Mock ($2^{-\Delta\Delta Ct}$)
IRF1 IRF3 IRF7 IRF9
B
DMSO
CsA
3 h
4 h
● DMSO
▲ CsA
IRF1 expression [%]
***
***
3 h
4 h
C
relative mRNA level [%]
**
ns
**
***
ns
***
IFNL1
IFNL2/3
● CsA only ▲ CsA+scr siRNA ◘ CsA+IRF1 siRNA
D
relative IFNλ protein release [%]
*
ns
*
-
scr siRNA
IRF1 siRNA
CsA

Figure 6.

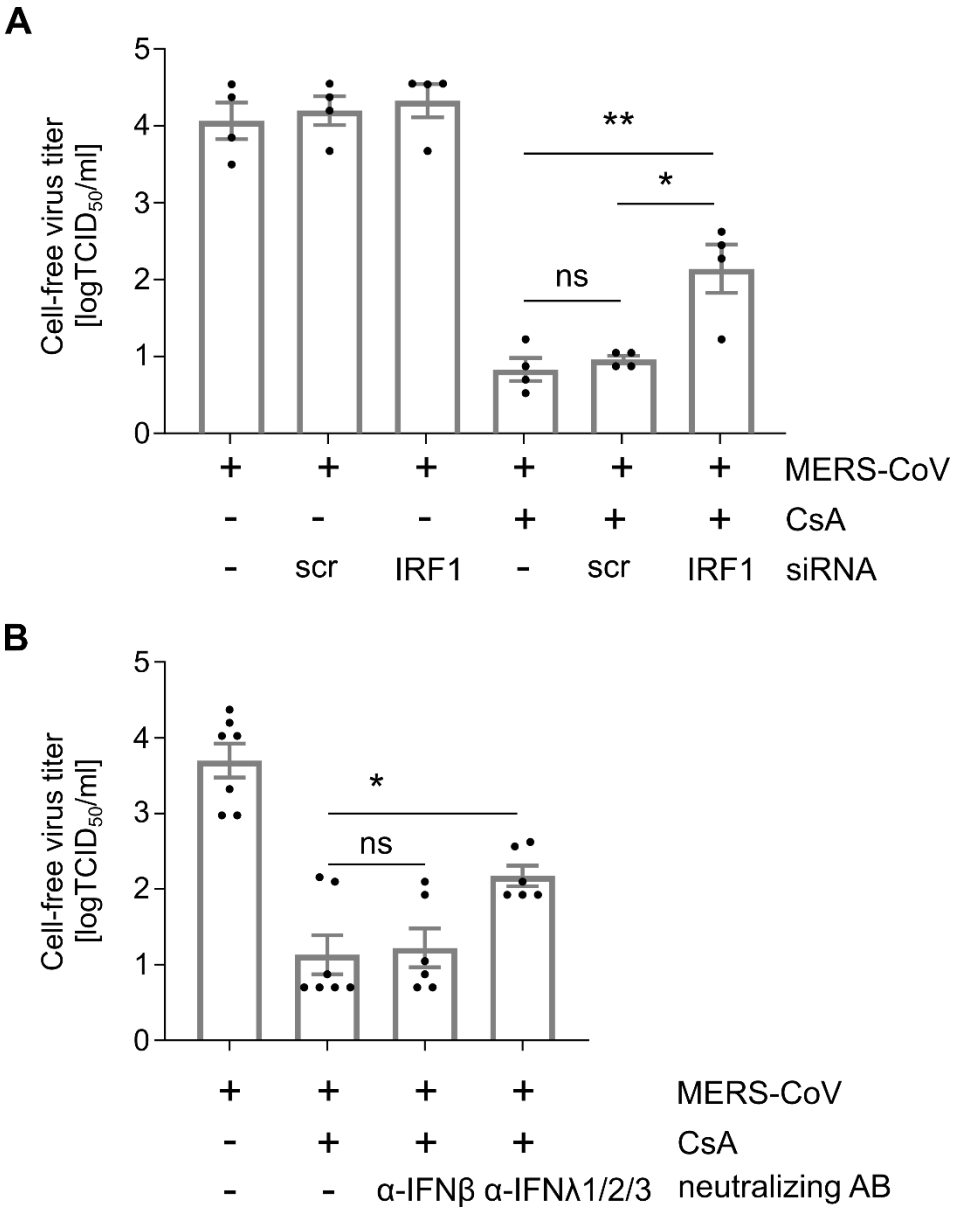
A
Cell-free virus titer [logTCID50/ml]
5
4
3
2
1
0
**
*
ns
+ + + + + + MERS-CoV
- - - + + + CsA
- scr IRF1 - scr IRF1 siRNA
B
Cell-free virus titer [logTCID50/ml]
5
4
3
2
1
0
*
ns
+ + + + MERS-CoV
- + + + CsA
- - α-IFNβ α-IFNλ1/2/3 neutralizing AB

Figure 7.

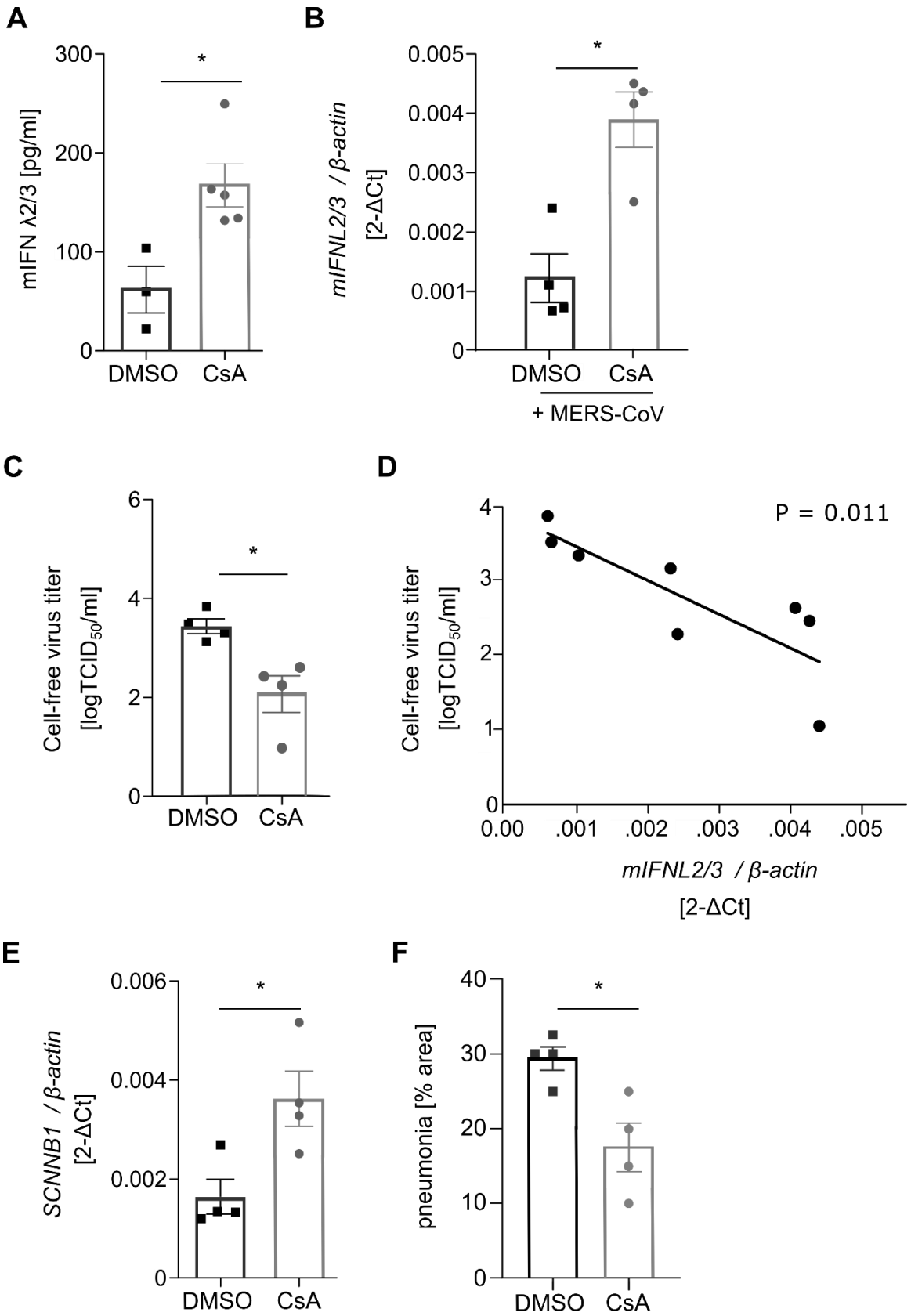
A
mIFN λ2/3 [pg/ml]
300
200
100
0
*
DMSO
CsA
B
mIFNL2/3 / β-actin
[2-ΔCt]
0.005
0.004
0.003
0.002
0.001
0
*
DMSO
CsA
+ MERS-CoV
C
Cell-free virus titer
[logTCID50/ml]
6
4
2
0
*
DMSO
CsA
D
P = 0.011
Cell-free virus titer
[logTCID50/ml]
4
3
2
1
0
0.00
.001
.002
.003
.004
.005
mIFNL2/3 / β-actin
[2-ΔCt]
E
SCNNB1 / β-actin
[2-ΔCt]
0.006
0.004
0.002
0
*
DMSO
CsA
F
pneumonia [% area]
40
30
20
10
0
*
DMSO
CsA

Figure 8.

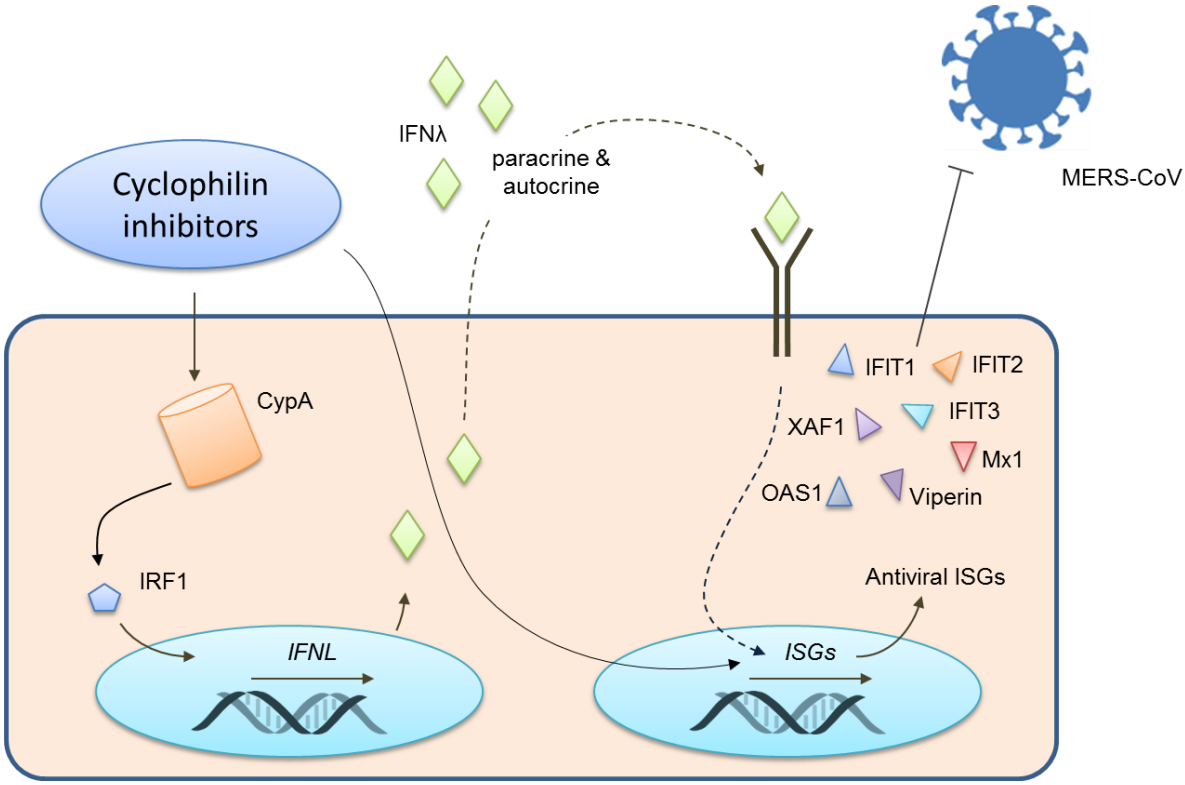
IFNλ
paracrine &
autocrine
MERS-CoV
Cyclophilin
inhibitors
CypA
IRF1
IFNL
ISGs
IFIT1
IFIT2
IFIT3
XAF1
Mx1
OAS1
Viperin
Antiviral ISGs

Online Supplement

Methods

Cell lines, primary alveolar epithelial cells and stimulation studies

Calu-3 cells used for infection and stimulation experiments and VeroE6 cells used for virus titration were cultivated using DMEM/F12 with 10% FCS or DMEM with 10% FCS. AEC and Calu-3 cells were treated with the following reagents: 10 µM Cyclosporin A (CsA, Sigma Aldrich), 10 µM Alisporivir (ALV, Debiopharm), 20 µM calcineurin inhibitory peptide (CIP, Tocris), 10 µM SB203580 (Tocris), 10 µM SP600125 (Sigma Aldrich), 50 µM NFAT-inhibitor (Cayman Chemical Company), DMSO solvent control or H_2O only (for CIP, exclusively).

Neutralization studies

MERS-CoV-infected Calu-3 cells were stimulated with CsA and treated with neutralizing antibodies against IFNλ1 (100 % cross-reactivity with IFNλ3) and IFNλ2 (R&D, 4 or 5 µg/ml, respectively). Neutralizing antibodies against IFNβ were used as a control (R&D, 4 µg/ml). At 24 h pi, cell culture supernatants were harvested for $TCID_{50}$ titration.

siRNA transfection

Silencer® Select siRNA against IRF1 (ID s7503, Invitrogen) and Silencer® Select Negative Control #1 siRNA (Invitrogen) were used for knock down studies. Calu-3 cells were transfected using Oligofectamine Transfection Reagent (Invitrogen) according to the manufacturer's protocol. 4 h post transfection (pt), cells were

stimulated with CsA and IFN-release and IFN-mRNA induction were analyzed 15 h post stimulation. For infection studies, IRF1-knockdown cells were infected 15 h pt with MERS-CoV, stimulated with CsA one hour after viral adsorption and analyzed for viral release and replication 24 h pi.

RNA extraction, cDNA synthesis and quantitative Real-Time-PCR

Total RNA was isolated using RNeasy-Minikit (Qiagen) followed by cDNA synthesis with random hexamer primers and RevertAid H Minus First Strand cDNA Synthesis Kit (ThermoFisher). Quantitative Real-Time-PCR (qPCR) using 50 ng cDNA in a total volume of 25 µl with 2× QuantiFast SYBR green PCR Master Mix (Applied BioSystems) and 100 nM of forward and reverse primers (table 1) was performed (StepOne Real-Time PCR System (Applied Biosystems). ß-Actin served as housekeeping gene for normalization. For determination of viral replication in cell cultures E-gene mRNA per actin ($2^{-\Delta ct}$) was calculated. Changes in *IFN*, *IRF* and *ISG* RNA levels were determined in fold change over mock ($2^{-\Delta\Delta Ct}$) [1].

Quantification of viral RNA in lung homogenate was performed as described by Malczyk et al. 2015 [2]. Lung samples were taken from the center of the left lung lobe and were homogenized in 1 ml DMEM with ceramic beads (Lysing Matrix H 500, 2ml tube, MP Biomedicals) in a mixer mill (Retsch Schwingmühle MM 400) for 10 min at 30 Hz. To remove tissue debris, homogenates were centrifuged for 10 min at 2,400 rpm. Live virus particles in supernatant (in $TCID_{50}$ per milliliter) were determined on VeroE6 cells. 100 µl of the supernatants were used for RNA isolation with the RNeasy minikit (Qiagen) according to the manufacturer's instructions. The amount of RNA was measured with a NanoDrop ND-100 spectrophotometer. Total RNA was reverse transcribed and quantified by real-time PCR using the SuperScript III

OneStep RT-PCR System (Invitrogen Life Technologies) as described previously [2, 3].

Primers used in this study (all 5' to 3')

MERSupE for: GCAACGCGCGATTCAGTT, rev: GCCTCTACACGGGACCCATA

Mouse beta-Actin for: TAGCACCATGAAGATCAAGAT, rev: CCGATCCACACAGAGTACTT

Mouse IFN-λ2/3 for: AGCTGCAGGTCCAAGAGCG, rev: GGTGGTCAGGGCTGAGTCATT

Mouse SCNN1B for: TGGTACTGCAATAACACCAACAC, rev:

AGCAGCGTAAGCAGGAACC

hActin for: CTGGGAGTGGGTGGAGGC, rev: TCAACTGGTCTCAAGTCAGTG

hIRF1 for: AGGAGCCAGATCCCAAGACGTG, rev: AGCATCCGGTACACTCGCACAG

hIFIT2 for: CTGCAACCATGAGTGAGAACAA, rev CCTCCATCAAGTTCCAGGTGAA

hIFNλ1 for: CGCCTTGGAAGAGTCACTCA; rev: GAAGCCTCAGGTCCCAATTC

hIFNλ2/3 for: GCCAAAGATGCCTTAGAAGAG, rev: CAGAACCTTCAGCGTCAGG

hIFN-β for: TGCCTCAAGGACAGGATGAAC; rev: GGAACTGCTGCAGCTGCTTA

hIFIT1 for: CAGCAACCATGAGTACAAAT, rev: AAGTGACATCTCAATTGCTC

hOAS for : GCCCTGGGTCAGTTGACTGG, rev: TGAAGCAGGTGGAGAACTCGC

hMXA for: CGGTCCTCAGCCTGGTAG, rev: TGGGGGTCCCGAGATATT

hViperin for: TGCCACAATGTGGGTGCTTACAC, rev: CTCAAGGGGCAGCACAAAGGAT

hIFIT3 for: GAACATGCTGACCAAGCAGA, rev: CAGTTGTGTCCACCCTTCCT

hXAF1 for: CTTACTGCCTGCGGTTCCTG, rev: CGTACACCCAACCTGCTGGT

hIRF3 for: ACC AGC CGT GGA CCA AGAG, rev: TAC CAA GGC CCT GAG GCA C

hTetherin for: CCG TCCTGCTCGGCTTT, rev: CCGCTCAGAACTGATGAGATCA

hIRF7 for: GAGACTGGCTATTGGGGGAG, rev: GACCGAAATGCTTCCAGGG

hIRF 9 for: TTCTGTCCCTGGTGTAGAGCCT, rev: TTTCAGGACACGATTATCACGG

IFNλ 1/3 ELISA

Quantification of released human IFNλ1/3 in the supernatant of CsA-stimulated cells or murine IFNλ 2/3 in the bronchoalveolar lavage of CsA-fed mice was performed with DuoSet® Ancillary Reagent Kit 2 and human IFN-lambda 1/3 or mouse IFN-lambda 2/3 DuoSet ELISA (all R&D) according to the manufacturer's protocol.

IRF1 indirect immunofluorescence analysis

Intracellular localization of endogenous IRF1 protein was analyzed 3 and 4 hour post CsA stimulation. DMSO-treated cells were used as negative control. Stimulated cells were fixed with 4% PFA and permeabilized with methanol/acetone for 10 min. Cells were incubated with a rabbit monoclonal-anti-IRF1 (1:100; Cell Signaling) and an AlexaFluor 594-conjugated secondary antibody (1:400; Dianova). Cell nuclei were counterstained with DAPI. The samples were mounted in Fluoprep (Biomérieux) and images were recorded with a confocal laser scanning microscope (Leica SP5).

Epithelial integrity measurements

Calu3 cells were seeded in 0.4µm pore size transwell cell culture dishes (Corning) and cultured until achieving electrochemical resistances (TER) of ≥800Ω /cm^2 as measured by Millicell-ERS2 device. Cells were infected apically with MERS-CoV at MOI 0.1 and treated with CsA, ALV and JNK for 24 h at 37°C and then supplied with 3 mg/ml 70kDa FITC-dextran (Sigma Aldrich) labeled cell culture media including selected inhibitors. After 24 h of incubation at 37°C, apical and basal media were analyzed for FITC-dextran concentration (multi-mode-reader Synergy LX, Bio-Tek Instruments). Vectorial water transport was calculated by changes in FITC-dextran

concentration between apical (C_a) and basal (C_b) media in comparison to starting conditions (C_0): [1 - (C_0/C_a)] - [1 - (C_0/C_b)]; as reported previously [4].

Apoptosis quantification

For quantification of MERS-CoV induced apoptosis a Caspase 3/7 Gloassay® (Promega) was performed according to the manufacturer's protocol. Confluent Calu-3 cells were infected and treated as describes above. 24 h pi Caspase 3/7 Globuffer was added to the same amount of cell supernatant (in total 300 µl) and incubated for 30 min. 100 µl of supernatant was pipetted into a whitewall 96 well plate and luminescence was analyzed using Centro LB 960 (Berthold Technologies). Duplicate determination was performed and Globuffer alone and supernatant without Globuffer were analyzed for subtraction of background. Shown are relative units to uninfected and DMSO-treated control-cells (set as 1).

Western blot

SDS-Page and western blot was analyzed as described previously [5]. Calu-3 cells were infected with MERS-CoV using a MOI of 0.1 and stimulated with CsA 1 hour after virus adsorption. 24 h pi cells were scratched off with 500 µl PBS supplemented with protease-inhibitor mix (Calbiochem) and centrifuged for 5 min at 5,000 rpm. Cell pellets were resuspended in sample buffer [6] containing 4% SDS and boiled at 100°C for 10 min. After discharge of the probes out of the BSL4 laboratory another 10 min boiling step was performed before the samples were separated using an 7,5 % SDS-Gel. After blotting on a nitrocellulose membrane and blocking using PBSdef with 5% milk powder first antibodies (Anti-CFTR Antibody, clone MM13-4 and mouse monoclonal Anti-Vinculin antibody both Sigma-Aldrich; ENaCβ antibody (E-10), sc-48428; Santa Cruz Biotechnology) diluted in PBSdef with

1% milk powder were incubated overnight followed by secondary antibody-incubation for 1 h (Goat Anti-Mouse/HRP and Swine Anti-Rabbit/HRP; both Dako). For visualization of the signals Image Lab software was used.

Mouse in vivo experiments - sample preparation

All animal experiments were performed in accordance with the regulations of German animal protection laws and as authorized by the regional authorities (Regierungspräsidium Giessen, G73/2017). Six- to 12-week-old C57Bl/6J mice were inoculated intratracheally (i.t.) with 50 µl of an adenovirus vector encoding human DPP4 and mCherry with a final titer of 2.5×10^8 PFU per inoculum (AdV-hDPP4; ViraQuest Inc.). Starting at day 3 post transduction, mice were fed daily with CsA (50mg/kg/day) or with DMSO as control mixed with nut-chocolate creme. CsA or DMSO fed mice were challenged intranasally (i.n.) with 30 µl of MERS-CoV at a dose of 1.5×10^5 TCID50 as described before [2, 3]. The mice were euthanized 4 or 7 days after MERS-CoV infection, and representative left lobe lung samples were prepared for RNA isolation.

Non-infected control mice were fed with CsA or DMSO for 6 days and bronchoalveolar lavage was performed to determine the IFNλ levels in the lung by ELISA according to manufacturer's instructions (Mouse IL-28A/B (IFN-lambda 2/3) ELISA with R&D Systems DuoSet Development Kit).

Histology

For histopathological analyses of formalin-fixed, paraffin-embedded murine lung tissues, sections of 2 µm thickness were cut from four to six evenly distributed planes throughout the entire lungs and mounted on adhesive glass slides. The slides were stained with hematoxylin and eosin and coverslipped. Histopathological evaluation

was performed using an established four grade scoring scheme [7] including the following parameters: affected area, severity and distribution of interstitial inflammation, infiltration of macrophages, lymphocytes and granulocytes, necrosis, alveolar hemorrhage and edema as well as formation of Bronchus-associated lymphoid tissue (BALT) and perivascular, lymphocytic cuffing.

Supplemental Figures

Figure E1: ENaCβ expression in Calu-3 after MERS-CoV infection and CsA treatment. Calu-3 were infected with MERS-CoV using an MOI of 0.1, stimulated with DMSO or 10 µM Cyclosporin A (CsA), and analyzed at 24h pi. Cell lysates were analyzed by western Blot for expression of ENaCβ (100 kDa) and vinculin (120 kDa). Left panel shows representative western blots of n = 3 experiments. Right panel shows relative quantitation with mock samples set to 100%.

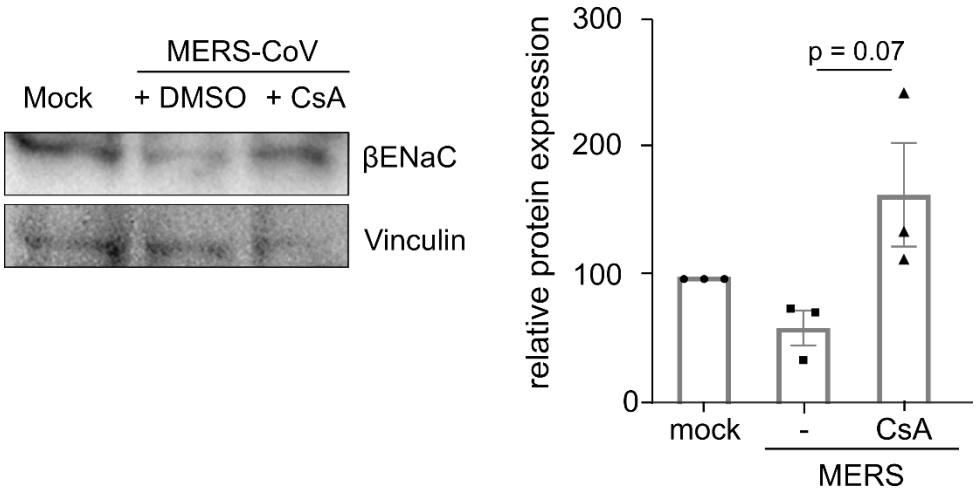

Figure E2: ALV treatment improves epithelial integrity upon MERS-CoV infection. Calu-3 were infected with MERS-CoV using an MOI of 0.1, stimulated with DMSO or 10 µM CsA or 10 µM ALV, and analyzed at 24h pi. (**A**) MERS-CoV-induced CPE and foci formation was documented in live cells by phase contrast microscopy at a magnification of 100x. (**B**) Epithelial integrity was quantified by transepithelial resistance measurements (**C**) and vectorial water transport evaluated by FITC-Dextran quantification 48h pi. Bar graphs in (**B, C**) represent means ±SEM of n = 4 experiments. Statistical significance was analyzed by one-way-ANOVA and Bonferroni's multiple comparisons test, where all groups were compared to each

other. *P < 0.05; **P < 0.01. Shown micrographs (**A**) are representative of n = 3 - 4 experiments.

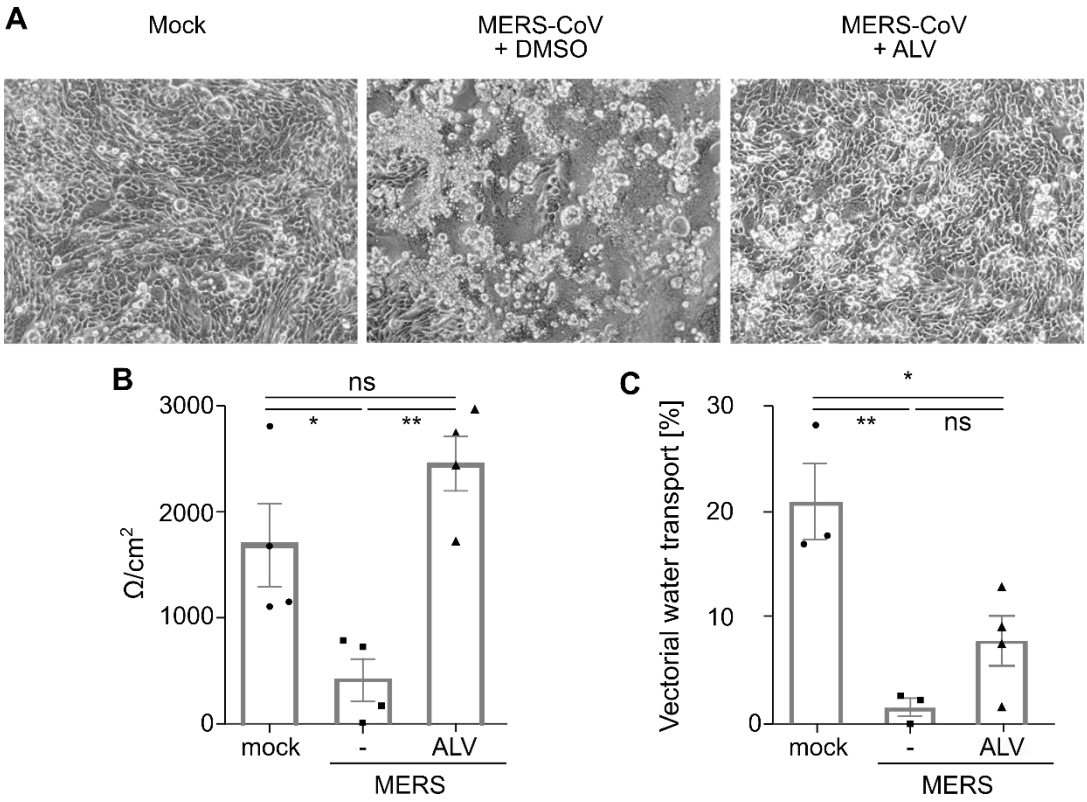

Figure E3: Inhibition of JNK does not affect cell foci formation or epithelial integrity. Calu-3 were infected with MERS-CoV using an MOI of 0.1, stimulated with DMSO or 10 µM JNK inhibitor (SP600125), and analyzed at 24h pi. (**A**) MERS-CoV-induced CPE and foci formation was documented in live cells by phase contrast microscopy at a magnification of 100x. (**B**) Epithelial integrity was quantified by transepithelial resistance measurements (**C**) and vectorial water transport evaluated by FITC-Dextran quantification 48h pi. Bar graphs in (**B, C**) represent means ± SEM of n = 3 - 4 experiments. Statistical significance was analyzed by one-way-ANOVA and Bonferroni's multiple comparisons test, where all groups were compared to each other. *P < 0.05. Shown micrographs (**A**) are representative of n = 3 - 4 experiments.

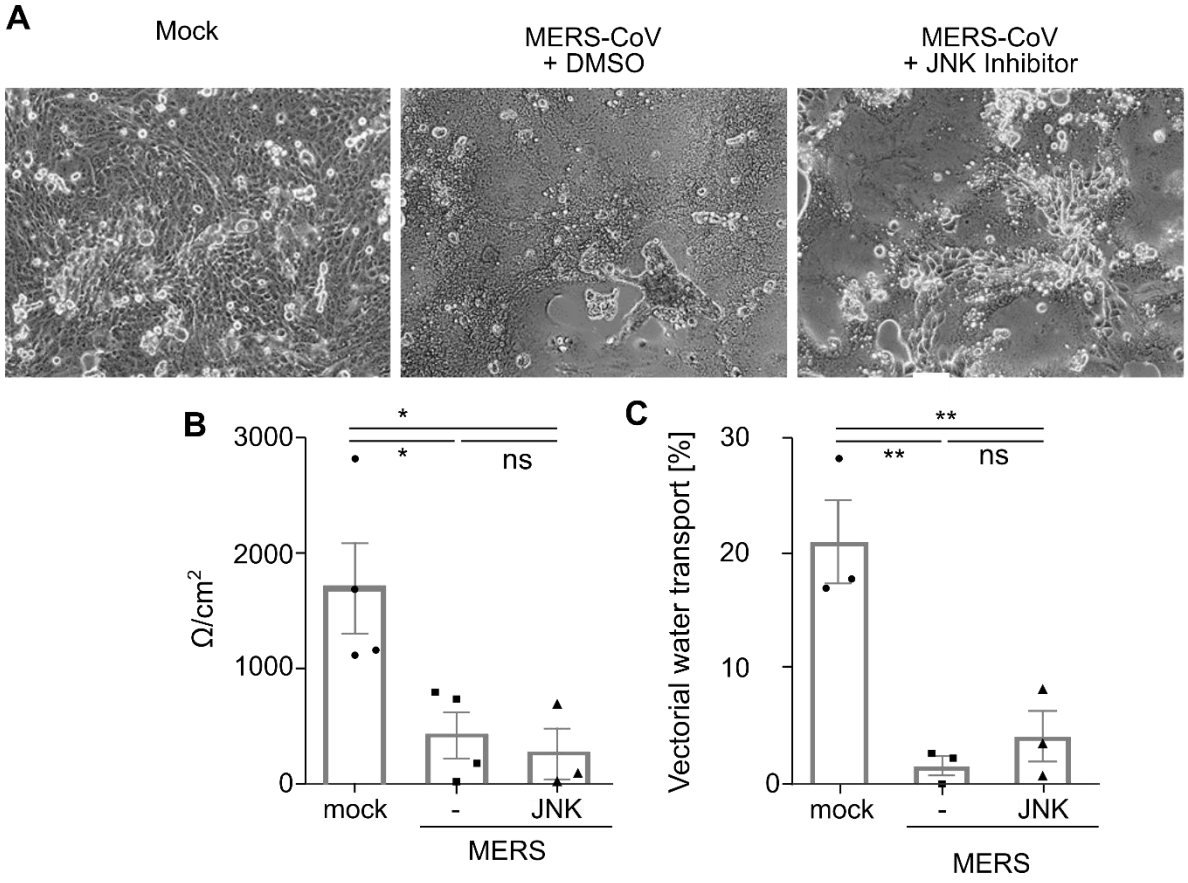

Figure E4: ALV induces interferon lambda to a similar extent as CsA. Calu-3 cells were stimulated with 10 µM Alisporivir or 10 µM CsA for 18, 24, 48 h, and 72 h, respectively. The amount of released IFNλ was measured by IFNλ1/3 ELISA (R&D Systems DuoSet Development Kit). Bar graphs represent mean ± SEM of n = 3 - 4 experiments.

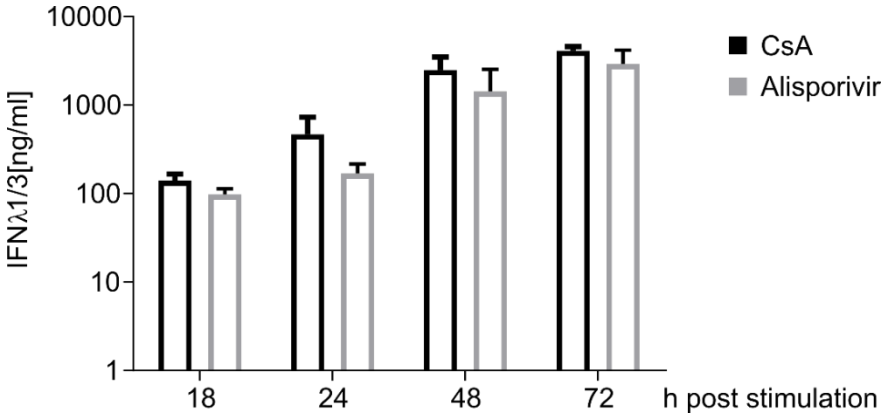

Figure E5: CsA serum levels after oral CsA application *in vivo*. Mice were fed daily with 50 mg/kg/day CsA for 6, 9 or 12 days. CsA serum levels were determined from blood sera by mouse Cyclosporin A ELISA-Kit (MyBioSource) according to the manufacturer's protocol. Single data points and means ± SEM are given.

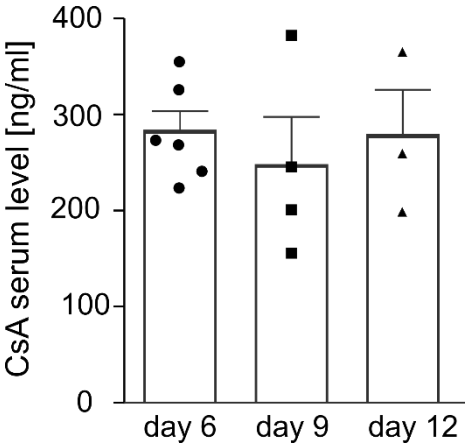

Figure E6: mCherry expression levels after oral CsA application *in vivo*. The amount of mCherry was determined as an evidence for successful and stable hDPP4 transduction. Mice were intratracheally infected with recombinant adenovirus encoding for human DPP4 and mCherry (Ad-hDPP4). Oral application of CsA (50 mg/kg/day) or DMSO as solvent control was started at day 3 post transduction, while mice were infected with $1.5x10^5$ $TCID_{50}$/ml MERS-CoV via the intranasal route at day 5 post transduction. Mice were euthanized and lungs were isolated 4 days post MERS-CoV infection. mCherry RNA content was analyzed from lung homogenates using OneStep RT-PCR kit as described previously [2, 3]. Quantification was carried out using a standard curve based on 10-fold serial dilutions of appropriately cloned RNA ranging from 10^2 to 10^5 copies. Bar graphs in represent mean ± SEM of n = 4 - 6 experiments.

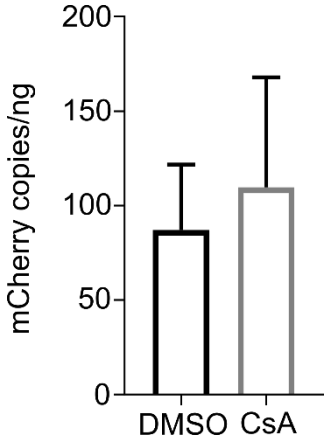

Figure E7: CsA induces interferon lambda and restricts MERS-CoV mRNA expression at day 4 pi *in vivo.* Mice were intratracheally infected with recombinant adenovirus encoding for human DPP4 and mCherry (Ad-hDPP4). Oral application of CsA (50mg/kg/day) or DMSO as solvent control was started at day 3 post transduction, while mice were infected with $1.5x10^5$ $TCID_{50}$/ml MERS-CoV via the intranasal route at day 5 post transduction. Mice were euthanized and lungs were isolated 4 days post MERS-CoV infection. Lung homogenate was used to quantify (**A**) viral load by $TCID_{50}$. Bar graphs represent means ± SEM of n = 6 - 8 experiments. Statistical significance was calculated using student's t-test. *P < 0.05. In (**B**) correlation between MERS-CoV titers and IFNλ2/3 mRNA expression levels was calculated using Pearson correlation efficient.

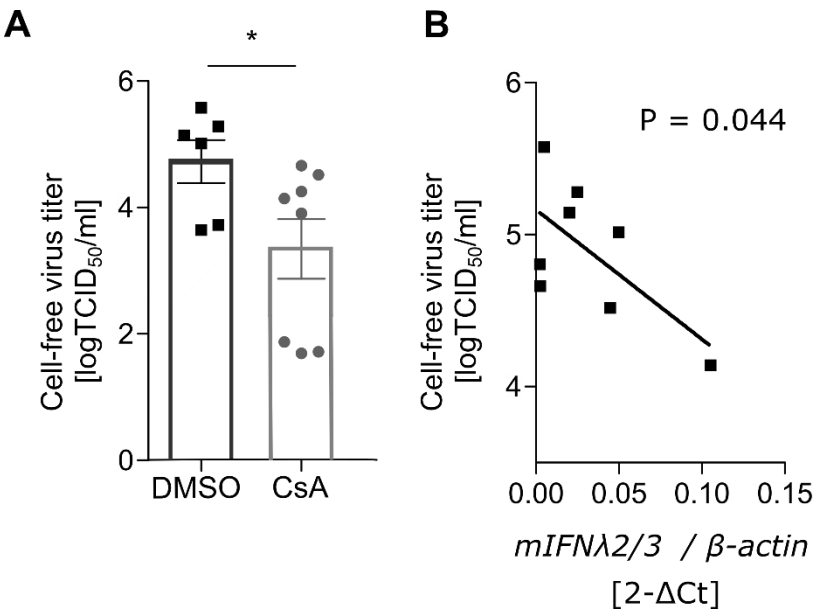

Figure E8: CsA prevents extensive edema formation in MERS-CoV-infected mice. Mice were intratracheally infected with recombinant adenovirus encoding for human DPP4 and mCherry (Ad-hDPP4). Oral application of CsA (50mg/kg/day) or DMSO as solvent control was started at day 3 post transduction, while mice were infected with $1.5x10^5$ $TCID_{50}$/ml MERS-CoV via the intranasal route at day 5 post transduction. Mice were euthanized and lungs were isolated 7 days post MERS-CoV infection. Fixed lungs were processed for histology as described and stained with H&E. Extensive alveolar edema formation was only apparent in DMSO-treated mice (upper panel), while only mildly to moderately seen in CsA-treated mice (lower panel).

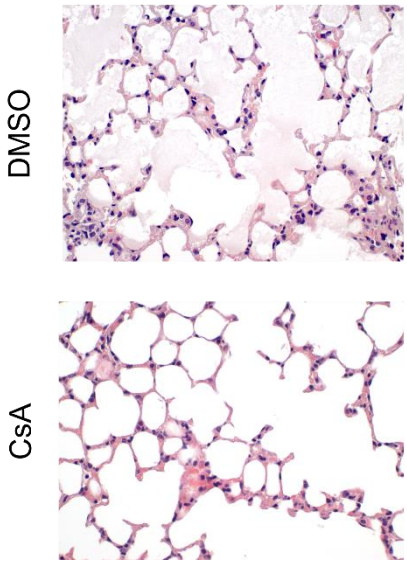

Supplemental Literature

1. Sauerhering L, Müller H, Behner L, Elvert M, Fehling SK, Strecker T, Maisner A. Variability of interferon-λ induction and antiviral activity in nipah virus infected differentiated human bronchial epithelial cells of two human donors. *J. Gen. Virol.* 2017; .

2. Malczyk AH, Kupke A, Prüfer S, Scheuplein VA, Hutzler S, Kreuz D, Beissert T, Bauer S, Hubich-Rau S, Tondera C, Eldin HS, Schmidt J, Vergara-Alert J, Süzer Y, Seifried J, Hanschmann K-M, Kalinke U, Herold S, Sahin U, Cichutek K, Waibler Z, Eickmann M, Becker S, Mühlebach MD. A Highly Immunogenic and Protective Middle East Respiratory Syndrome Coronavirus Vaccine Based on a Recombinant Measles Virus Vaccine Platform. Perlman S, editor. *J. Virol.* [Internet] 2015 [cited 2019 Jul 19]; 89: 11654–11667Available from: http://www.ncbi.nlm.nih.gov/pubmed/26355094.

3. Volz A, Kupke A, Song F, Jany S, Fux R, Shams-Eldin H, Schmidt J, Becker C, Eickmann M, Becker S, Sutter G. Protective Efficacy of Recombinant Modified Vaccinia Virus Ankara Delivering Middle East Respiratory Syndrome Coronavirus Spike Glycoprotein. Perlman S, editor. *J. Virol.* [Internet] 2015 [cited 2019 Jan 10]; 89: 8651–8656Available from: http://www.ncbi.nlm.nih.gov/pubmed/26018172.

4. Peteranderl C, Morales-Nebreda L, Selvakumar B, Lecuona E, Vadász I, Morty RE, Schmoldt C, Bespalowa J, Wolff T, Pleschka S, Mayer K, Gattenloehner S, Fink L, Lohmeyer J, Seeger W, Sznajder JI, Mutlu GM, Budinger GRS, Herold S, Jain S, Short K, Kroeze E, Fouchier R, Kuiken T, Kuiken T, Taubenberger J, Herold S, Matthay M, Ware L, Zimmerman G, et al. Macrophage-epithelial paracrine crosstalk inhibits lung edema clearance during influenza infection. *J. Clin. Invest.* [Internet] American Society for Clinical Investigation; 2016 [cited 2016 Sep 11]; 126: 1566–1580Available from: https://www.jci.org/articles/view/83931.

5. Tamakatsu Y, Krähling V, Kolesnikova L, Halwe S, Lier C, Baumeister S, Noda T, Biedenkopf N, Becker S. Serine-Arginine Protein Kinase 1 Regulates Ebola Virus Transcription. *MBio* [Internet] 2020; 11: e02565-19Available from: https://www.ncbi.nlm.nih.gov/pubmed/32098814.

6. Kolesnikova L, Berghofer B, Bamberg S, Becker S. Multivesicular Bodies as a Platform for Formation of the Marburg Virus Envelope. *J. Virol.* 2004; .

7. Dietert K, Gutbier B, Wienhold SM, Reppe K, Jiang X, Yao L, Chaput C, Naujoks J, Brack M, Kupke A, Peteranderl C, Becker S, von Lachner C, Baal N, Slevogt H, Hocke AC, Witzenrath M, Opitz B, Herold S, Hackstein H, Sander

LE, Suttorp N, Gruber AD. Spectrum of pathogen- and model-specific histopathologies in mouse models of acute pneumonia. Jeyaseelan S, editor. *PLoS One* [Internet] 2017 [cited 2019 Jan 10]; 12: e0188251Available from: http://www.ncbi.nlm.nih.gov/pubmed/29155867.